

A new technique to incorporate multiple fermion flavors in tensor renormalization group method for lattice gauge theories

Atis YOSPRAKOB^{1)*}, Jun NISHIMURA^{2,3)†} and Kouichi OKUNISHI^{1)‡}

¹⁾*Department of Physics, Niigata University,
Niigata 950-2181, Japan*

²⁾*KEK Theory Center, Institute of Particle and Nuclear Studies,
High Energy Accelerator Research Organization,
1-1 Oho, Tsukuba, Ibaraki 305-0801, Japan*

³⁾*Graduate Institute for Advanced Studies, SOKENDAI,
1-1 Oho, Tsukuba, Ibaraki 305-0801, Japan*

Abstract

We propose a new technique to incorporate multiple fermion flavors in the tensor renormalization group method for lattice gauge theories, where fermions are treated by the Grassmann tensor network formalism. The basic idea is to separate the site tensor into multiple layers associated with each flavor and to introduce the gauge field in each layer as replicas, which are all identified later. This formulation, after introducing an appropriate compression scheme in the network, enables us to reduce the size of the initial tensor with high efficiency compared with a naive implementation. The usefulness of this formulation is demonstrated by investigating the chiral phase transition and the Silver Blaze phenomenon in 2D Abelian gauge theories with N_f flavors of Wilson fermions up to $N_f = 4$.

*E-mail address : ayosp(at)phys.sc.niigata-u.ac.jp

†E-mail address : jnishi(at)post.kek.jp

‡E-mail address : okunishi(at)phys.sc.niigata-u.ac.jp

1 Introduction

Nonperturbative computation in fermionic systems has always been challenging due to the anti-commuting nature of Grassmann variables. In Monte Carlo methods, the Grassmann variables have to be integrated out first, yielding the fermion determinant $\det M$, which makes the computation very time-consuming since the matrix M has a size proportional to the system size V . While the computational cost can be made $O(V)$ by using the pseudo-fermion technique with an appropriate Hybrid Monte Carlo algorithm, the calculation is still typically a few orders of magnitude more time-consuming than corresponding bosonic systems. Moreover, in many interesting fermionic systems such as finite density systems, strongly-correlated electron systems, and theories with chiral fermions, the fermion determinant becomes complex, which causes the notorious sign problem in conventional Monte Carlo methods. In order to overcome this problem, various methods such as the complex Langevin method [1, 2, 3, 4, 5], the Lefschetz thimble method [6, 7, 8, 9, 10, 11, 12], and the density of state method [13, 14, 15] have been developed. However, each method has its pros and cons, and many models still remain out of reach.

All these problems associated with fermionic systems can be solved beautifully in the tensor network method [16, 17, 18, 19, 20, 21, 22, 23, 24, 25, 26, 27, 28, 29], which is not a statistical approach based on important sampling. This method was first introduced to handle many-body systems in condensed matter physics with the main application to the calculation of the ground state based on the variational principle [30, 31, 32, 33, 34, 35]. However, it can also be used to directly compute the partition function with some procedures based on coarse-graining, which is similar in spirits to the real-space renormalization group and hence the name, “the tensor renormalization group (TRG) method”. Notably, it enables the computation of the partition function with a computational cost that grows only logarithmically with the system size. Although the original TRG method was proposed for a two-dimensional bosonic system [17], improved versions were subsequently developed [18, 19, 20, 29], and it has also been generalized to higher dimensional systems [21, 22, 23, 24] and to fermionic systems, where Grassmann variables are treated directly [25, 26, 27, 28, 24] unlike in Monte Carlo methods. Using this “Grassmann tensor network”, one does not have to deal with the fermion determinant, and furthermore, the sign problem does not exist in the method from the outset because it is not a statistical approach.

A recent achievement of the TRG method is its application to gauge theory, in particular in the parameter regions that are not accessible to Monte Carlo methods due to the sign problem. Notable examples include the 2D gauge theories with a θ term [36, 37, 38], 2D SU(2) gauge-Higgs model [39], one-flavor Schwinger model [27, 40, 41], 2D QCD [42], 3D

SU(2) gauge theory [43], 4D \mathbb{Z}_K gauge-Higgs models [44, 45] and so on. Among these applications, gauge theories with matter fields are of particular importance since typically they are not exactly solvable. However, the TRG method has so far been applied only to the case with one fermion flavor. When there are many flavors of fermions on a single lattice site, one encounters a problem that the size of the local Hilbert space, and thus the size of the initial tensor, grows exponentially with the number of flavors. This prevents us from studying theories with multiple flavors including QCD, which is a non-Abelian gauge theory with two (or three) flavors of light quarks.

In this paper, we propose a new technique that makes it possible to incorporate multiple flavors of fermions in gauge theory within the Grassmann tensor network formalism. The main idea is to separate the initial tensor into multiple layers associated with each flavor. Since the fermions with different flavors are interacting with the same gauge field, the interaction in the flavor direction becomes non-local after integrating out the gauge field. In order to avoid this problem, we introduce the gauge field in each layer as replicas and identify them all later. Once the system can be described by a tensor network, which is one dimension higher than the original theory due to the flavor direction, one can use the standard coarse-graining technique to compute the partition function. Our method is expected to be useful also in applying the TRG to the domain-wall formalism [46, 47] for chiral fermions regarding the flavor direction in our method as the extra space-time dimension. We also introduce an efficient compression scheme that further reduces the size of the initial tensor drastically, especially at large K . For $N_f = 1$, the performance of our method is found to be as good as in the previous calculations for the Schwinger model [27, 40, 41].

The usefulness of this formulation is demonstrated by applying it to Abelian gauge theories in two dimensions with N_f flavors of Wilson fermions. First, we investigate the chiral phase transition in the $N_f = 2$ case, which shows that the result obtained in the \mathbb{Z}_K gauge theory converges to the U(1) result obtained by using the Monte Carlo method [48] as we increase K . Next, we investigate the Silver Blaze phenomenon in the case of finite fermion density up to $N_f = 4$.

While this paper was being completed, we encountered a paper [49] which addresses the same issue of treating multiple fermion flavors in the TRG method. There the initial tensor for all the flavors is separated into multiple layers by using the matrix product decomposition, which requires the memory of order $O(e^{cN_f})$. In contrast, the memory cost of our method is of order $O(1)$ since the layers are separated analytically and all the layers are identical. This memory cost reduction enabled the investigation of gauge theories, which was not possible in Ref. [49].

The rest of this paper is organized as follows. In section 2, we explain our basic idea to implement multiple flavors in the TRG method. In particular, we derive the initial tensor for 2D Abelian gauge theories with Wilson fermions as an example. In section 3, we describe how we perform the procedures of the TRG method using the initial tensor. In particular, we discuss how we compress the initial tensor efficiently by inserting isometries and explain how we perform coarse-graining in the flavor space. In section 4, we present the numerical results obtained by our method. After showing some results of the performance tests concerning the initial tensor compression and the coarse-graining procedure in the flavor direction, we demonstrate the usefulness of our method by investigating the chiral phase transition and the Silver Blaze phenomenon in 2D Abelian gauge theories. Section 5 is devoted to a summary and discussions. In Appendix A, we give a brief review of the Grassmann tensor network. In Appendix B, we describe the coarse-graining algorithm in detail. In Appendix C, we discuss the generalization of our technique to a model with local multi-flavor interactions, which is important, in particular, in applying our method to the domain-wall formalism.

2 The basic idea to implement multiple flavors

In this section, we explain our basic idea to implement multiple flavors in the TRG method. First, we split the system into multiple layers by introducing replicas of gauge fields for each flavor, and then we construct the initial tensor based on the Grassmann tensor network formalism including the flavor direction.

2.1 Splitting the system into multiple layers

For simplicity, we will describe our idea in the case of Abelian gauge theory $G \subseteq U(1)$ on a two-dimensional square lattice Λ_2 with the lattice spacing a although it can be readily applied to higher dimensions and non-Abelian cases. The gauge field $A_{x,\mu}$ is represented on the lattice by the link variable $U_{x,\mu} = \exp(iaA_{x,\mu}) \equiv \exp(i\varphi_{x,\mu}) \in G$. Let us then consider the lattice action with N_f flavors of Wilson fermions given by

$$S = S_{\text{gauge}}[\varphi] + \sum_{x \in \Lambda_2} \sum_{\alpha=1}^{N_f} \bar{\psi}_x^{(\alpha)} \mathcal{D}^{(\alpha)} \psi_x^{(\alpha)} , \quad (2.1)$$

$$S_{\text{gauge}}[\varphi] = \beta \sum_{x \in \Lambda_2} \{1 - \cos(\varphi_{x,1} + \varphi_{x+1,2} - \varphi_{x+2,1} - \varphi_{x,2})\} , \quad (2.2)$$

$$\mathcal{D}^{(\alpha)} \psi_x^{(\alpha)} = -\frac{1}{2} \sum_{\nu=1,2} ((\mathbb{1} - \gamma_\nu) e^{+(\tilde{\mu}_\alpha \delta_{\nu,2} + iq_\alpha \varphi_{x,\nu})} \psi_{x+\hat{\nu}}^{(\alpha)} + (\mathbb{1} + \gamma_\nu) e^{-(\tilde{\mu}_\alpha \delta_{\nu,2} + iq_\alpha \varphi_{x-\hat{\nu},\nu})} \psi_{x-\hat{\nu}}^{(\alpha)})$$

$$+ (\tilde{m}_\alpha + 2) \psi_x^{(\alpha)} , \quad (2.3)$$

where $\beta = 1/(ga)^2$ is the inverse gauge coupling and γ_ν are the 2D gamma matrices given, for instance, by the Pauli matrices $\gamma_1 = \sigma_1$ and $\gamma_2 = \sigma_2$. The fermion fields are represented by the 2-component Dirac spinors $\psi_x^{(\alpha)}$ for each flavor α with charge q_α . We also introduce dimensionless chemical potential $\tilde{\mu}_\alpha$ and mass \tilde{m}_α for each flavor α .

Since fermions have $4N_f$ internal degrees of freedom, the local Hilbert space at a given lattice site has dimension $D = 2^{4N_f}$. Consequently, the size of the initial tensor grows as $D^4 = 2^{16N_f}$. It is thus beneficial to separate different flavors from each other to avoid the exponential growth of the tensor size with N_f . To that end, we split the link variables into N_f replicas and define the partition function as

$$Z = \int D\varphi \prod_{\alpha=1}^{N_f} (D\varphi^{(\alpha)} D\psi^{(\alpha)} D\bar{\psi}^{(\alpha)}) \delta(\varphi^{(\alpha)} - \varphi) e^{-\sum_\alpha S^{(\alpha)}} , \quad (2.4)$$

where the new action $S^{(\alpha)}$ is given as

$$S^{(\alpha)} = \frac{1}{N_f} S_{\text{gauge}}[\varphi^{(\alpha)}] + \sum_{x \in \Lambda_2} \bar{\psi}_x^{(\alpha)} \mathcal{D}^{(\alpha)} \psi_x^{(\alpha)} . \quad (2.5)$$

This enables us to split the Boltzmann weight into several layers corresponding to each replica, which are linked by the delta function. This decomposition into multiple layers has recently been considered in Ref. [49] but with the matrix product decomposition instead of using the delta function. Let us emphasize, however, that separating the layers by hand from the beginning as we do here is crucial in avoiding completely the singular value decomposition, which can be both memory-consuming and computationally expensive in lattice gauge theories.

While we have not introduced local interactions among different flavors, our tensor construction can be generalized to such cases as described in Appendix C.

2.2 Constructing the tensor network

We treat the fermion fields by the Grassmann tensor network [28] (See Appendix A for the details.). Let us rewrite the fermion action in the following form

$$\bar{\psi}_x^{(\alpha)} \mathcal{D}^{(\alpha)} \psi_x^{(\alpha)} = \bar{\psi}_x^{(\alpha)} W_x^{(\alpha)} \psi_x^{(\alpha)} + \sum_{\nu} \left(\bar{\psi}_x^{(\alpha)} H_{x,+\nu}^{(\alpha)} \psi_{x+\hat{\nu}}^{(\alpha)} + \bar{\psi}_x^{(\alpha)} H_{x,-\nu}^{(\alpha)} \psi_{x-\hat{\nu}}^{(\alpha)} \right) , \quad (2.6)$$

$$W_x^{(\alpha)} = \tilde{m}_\alpha + 2 , \quad (2.7)$$

$$H_{x,+\nu}^{(\alpha)} = -\frac{1}{2} (\mathbb{1} - \gamma_\nu) e^{+(\tilde{\mu}_\alpha \delta_{\nu,2} + i q_\alpha \varphi_{x,\nu}^{(\alpha)})} , \quad (2.8)$$

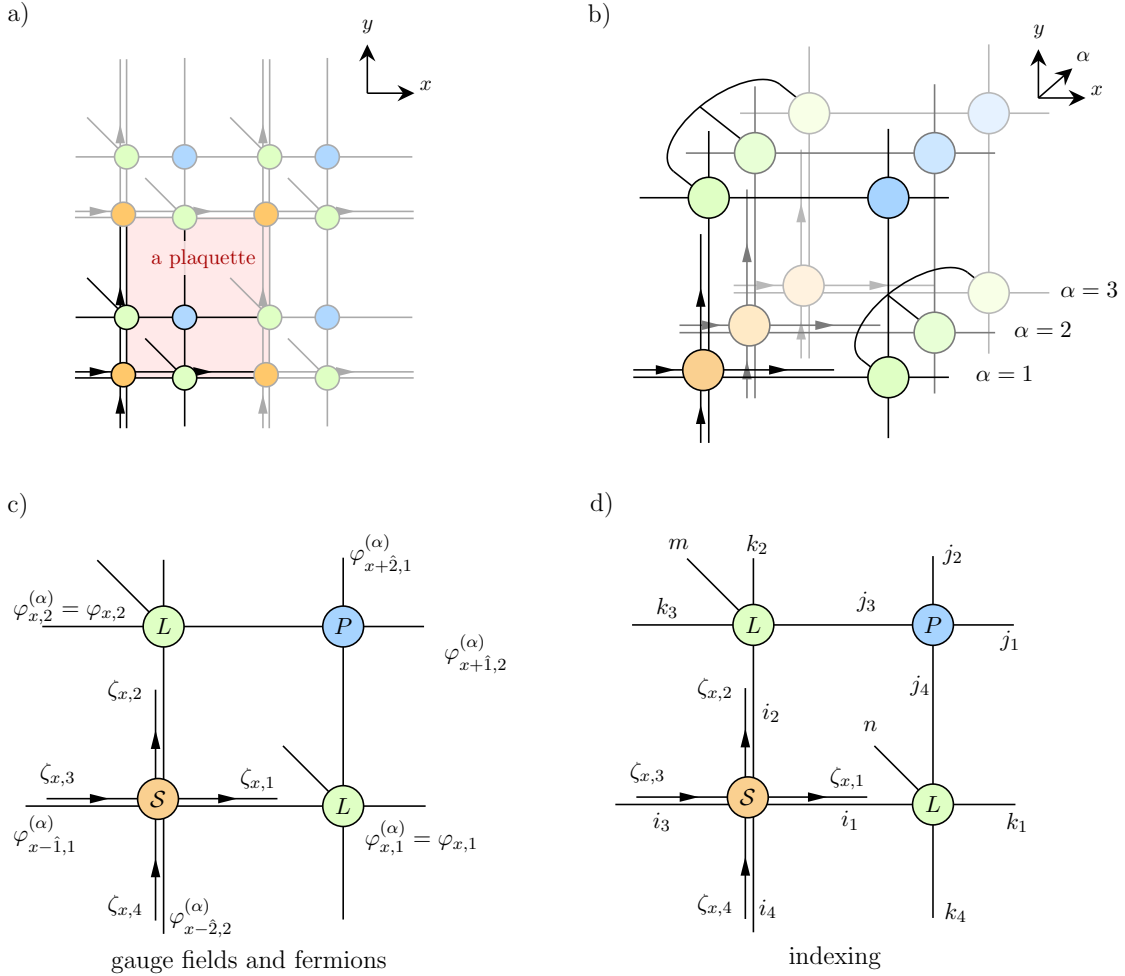


Figure 1: a) The two-dimensional tiling of the site tensor, which is composed of four subtensors. The shaded region represents a plaquette. b) The three-dimensional tiling of the site tensor for $N_f = 3$. Each layer corresponds to some flavor α . c) The site tensor (2.14) with the gauge fields and fermionic variables. d) The site tensor with the index for each bond. In the diagrams, fermionic legs with an arrow pointing away from the tensor are non-conjugated fermions, while those with an arrow pointing into the tensor are conjugated fermions.

$$H_{x,-\nu}^{(\alpha)} = -\frac{1}{2}(\mathbb{1} + \gamma_\nu) e^{-(\tilde{\mu}_\alpha \delta_{\nu,2} + iq_\alpha \varphi_{x-\hat{\nu},\nu}^{(\alpha)})} . \quad (2.9)$$

Here we transform the site fermions $(\psi, \bar{\psi})$ into auxiliary link fermions $(\eta, \bar{\eta})$ by using the relation¹

$$e^{-\bar{\psi}_x^{(\alpha)} H_{x,\pm\nu}^{(\alpha)} \psi_{x\pm\hat{\nu}}^{(\alpha)}} = \int d\bar{\eta}_{x,\pm\nu}^{(\alpha)} d\eta_{x,\pm\nu}^{(\alpha)} e^{-\bar{\eta}_{x,\pm\nu}^{(\alpha)} \eta_{x,\pm\nu}^{(\alpha)} - \bar{\psi}_x^{(\alpha)} \eta_{x,\pm\nu}^{(\alpha)} + \bar{\eta}_{x,\pm\nu}^{(\alpha)} H_{x,\pm\nu}^{(\alpha)} \psi_{x\pm\hat{\nu}}^{(\alpha)}} . \quad (2.10)$$

The integration of the link variables is performed by the summation

$$\int_{\mathbb{Z}_K} d\varphi f(\varphi) \equiv \sum_{k=1}^K w f(\varphi_k) \quad (2.11)$$

in the case of \mathbb{Z}_K gauge theory, where $w = 1/2\pi K$ and $\varphi_k = 2(k-1)\pi/K$. In the case of $U(1)$ gauge theory, we approximate the group integral by the Gaussian quadrature [36] as

$$\int_{U(1)} d\varphi f(\varphi) \equiv \int_{-\pi}^{+\pi} \frac{d\varphi}{2\pi} f(\varphi) \approx \sum_{k=1}^K w(\varphi_k) f(\varphi_k) , \quad (2.12)$$

where the weight function $w(\varphi)$ and the nodes φ_k depend on the quadrature.

Thus we arrive at

$$Z = \int_{\bar{\eta}\eta} \sum_{\{\varphi\}} \prod_{x,\alpha} \mathcal{T}_x^{(\alpha)} , \quad (2.13)$$

where we have defined the tensor

$$\mathcal{T}_x^{(\alpha)} = P_x^{(\alpha)} \mathcal{S}_x^{(\alpha)} L_{x,1}^{(\alpha)} L_{x,2}^{(\alpha)} , \quad (2.14)$$

$$P_x^{(\alpha)} = \left\{ w(\varphi_{x,1}^{(\alpha)}) w(\varphi_{x,2}^{(\alpha)}) \right\}^{1/N_f} e^{\frac{\beta}{N_f} \cos(\varphi_{x,1}^{(\alpha)} + \varphi_{x+1,2}^{(\alpha)} - \varphi_{x+2,1}^{(\alpha)} - \varphi_{x,2}^{(\alpha)})} , \quad (2.15)$$

$$L_{x,\mu}^{(\alpha)} = \delta(\varphi_{x,\mu}^{(\alpha)} - \varphi_{x,\mu}) . \quad (2.16)$$

$$\mathcal{S}_x^{(\alpha)} = \int d\psi_x^{(\alpha)} d\bar{\psi}_x^{(\alpha)} \exp \left[-\bar{\psi}_x^{(\alpha)} W_x^{(\alpha)} \psi_x^{(\alpha)} - \sum_{\pm,\nu} \left\{ \bar{\psi}_x^{(\alpha)} \eta_{x,\pm\nu}^{(\alpha)} - \bar{\eta}_{x\mp\hat{\nu},\pm\nu}^{(\alpha)} H_{x\mp\hat{\nu},\pm\nu}^{(\alpha)} \psi_x^{(\alpha)} \right\} \right] , \quad (2.17)$$

¹This follows from the identity

$$e^{-h\bar{\theta}\theta} = \int d\bar{\eta} d\eta e^{-\bar{\eta}\eta - \bar{\theta}\eta + h\bar{\theta}\theta}$$

for a Grassmann-even constant h and one-component Grassmann-odd numbers $\theta, \bar{\theta}, \eta, \bar{\eta}$, which can be generalized to the multi-component case in a straightforward manner.

and introduced a short-hand notation for the Grassmann integral

$$\int_{\bar{\eta}\eta} \equiv \int \prod_{x,\nu,\alpha} \left(d\bar{\eta}_{x,\nu}^{(\alpha)} d\eta_{x,\nu}^{(\alpha)} e^{-\bar{\eta}_{x,\nu}^{(\alpha)} \eta_{x,\nu}^{(\alpha)}} \right). \quad (2.18)$$

Note that the tensors P , L and \mathcal{S} are associated with the plaquettes, links, and sites, respectively. The connection of these tensors is shown in Fig. 1-c).

Performing the integral (2.17) symbolically², we obtain the tensor \mathcal{S} in the form of a polynomial of link fermions given as

$$\begin{aligned} \mathcal{S}_x^{(\alpha)} = & \sum_{\{I,J\}} (C_x^{(\alpha)})_{I_1 J_1 I_2 J_2 I_3 J_3 I_4 J_4} (\varphi_{x,1}^{(\alpha)}, \varphi_{x,2}^{(\alpha)}, \varphi_{x-\hat{1},1}^{(\alpha)}, \varphi_{x-\hat{2},2}^{(\alpha)}) \\ & \times \eta_{x,+1}^{I_1} \bar{\eta}_{x+\hat{1},-\hat{1}}^{J_1} \eta_{x,+2}^{I_2} \bar{\eta}_{x+\hat{2},-\hat{2}}^{J_2} \bar{\eta}_{x-\hat{1},+\hat{1}}^{I_3} \eta_{x,-1}^{J_3} \bar{\eta}_{x-\hat{2},+\hat{2}}^{I_4} \eta_{x,-2}^{J_4}, \end{aligned} \quad (2.19)$$

where the coefficient $C_x^{(\alpha)}$ depends on the gauge link variables. Here we have introduced

$$\eta^I \equiv \theta_1^{k_1} \theta_2^{k_2}, \quad (2.20)$$

$$I \equiv (k_1, k_2), \quad (2.21)$$

where θ_1 and θ_2 are the two components of η and $k_1, k_2 \in \{0, 1\}$ represent the occupation number of the components. Since some of these link fermions connect the same pair of sites, it is convenient to combine the fermion indices as $(I_a, J_a) \mapsto K_a$ with the prescription

$$\zeta_{x,1}^{K_1} = \eta_{x,+1}^{I_1} \bar{\eta}_{x+\hat{1},-\hat{1}}^{J_1}, \quad (2.22)$$

$$\zeta_{x,2}^{K_2} = \eta_{x,+2}^{I_2} \bar{\eta}_{x+\hat{2},-\hat{2}}^{J_2}, \quad (2.23)$$

$$\bar{\zeta}_{x,3}^{K_3} = (-)^{p(J_3)} \bar{\eta}_{x-\hat{1},+\hat{1}}^{I_3} \eta_{x,-1}^{J_3}, \quad (2.24)$$

$$\bar{\zeta}_{x,4}^{K_4} = (-)^{p(J_4)} \bar{\eta}_{x-\hat{2},+\hat{2}}^{I_4} \eta_{x,-2}^{J_4}, \quad (2.25)$$

where $p(J)$ is the Grassmann parity of the Grassmann number η^J defined by

$$p(J) = \sum_a j_a \quad (2.26)$$

with j_a being the fermion occupation number of the a -th component. The sign factor $(-)^{p(J)}$ is introduced for the consistency of Grassmann tensor contraction (See (A.17)-(A.18)).

Using the Grassmann index notation (A.1), the tensor \mathcal{S} can be expanded as (omitting the site index x to avoid redundancy)

$$\mathcal{S}_{\zeta_1 \zeta_2 \bar{\zeta}_3 \bar{\zeta}_4; i_1 i_2 i_3 i_4}^{(\alpha)} = \sum_{\{K\}} \mathcal{S}_{K_1 K_2 K_3 K_4; i_1 i_2 i_3 i_4}^{(\alpha)} \zeta_1^{K_1} \zeta_2^{K_2} \bar{\zeta}_3^{K_3} \bar{\zeta}_4^{K_4}, \quad (2.27)$$

²We use Mathematica v13.1.0.0 with a package for non-commutative algebra, NCAAlgebra v5.0.6.

$$S_{K_1 K_2 K_3 K_4; i_1 i_2 i_3 i_4}^{(\alpha)} = C_{I_1 J_1 I_2 J_2 I_3 J_3 I_4 J_4}^{(\alpha)}(\varphi_{i_1}^{(\alpha)}, \varphi_{i_2}^{(\alpha)}, \varphi_{i_3}^{(\alpha)}, \varphi_{i_4}^{(\alpha)}) (-)^{p(J_1)+p(J_2)} \quad (2.28)$$

with the sign factors given in (2.24) and (2.25). Here the index i in $\varphi_i^{(\alpha)}$ refers to the index of the quadrature node in (2.11). The site and orientation indices of the link variables $\varphi_{x,\mu}$ are omitted.

The tensor P can be rewritten in terms of the quadrature indices as

$$P_{j_1 j_2 j_3 j_4}^{(\alpha)} = \left\{ w(\varphi_{j_3}^{(\alpha)}) w(\varphi_{j_4}^{(\alpha)}) \right\}^{1/N_f} e^{\frac{\beta}{N_f} \cos(\varphi_{j_4}^{(\alpha)} + \varphi_{j_1}^{(\alpha)} - \varphi_{j_2}^{(\alpha)} - \varphi_{j_3}^{(\alpha)})} . \quad (2.29)$$

The tensor L (2.16), which depends on two fields, has actually five legs because it is connected to two plaquettes, two sites, and to the global gauge field $\varphi_{x,\mu}$. Therefore, it can be written in terms of the quadrature indices as

$$L_{i_\mu i_\nu k_\mu k_\nu m} = \delta_{m i_\mu} \delta_{m i_\nu} \delta_{m k_\mu} \delta_{m k_\nu} . \quad (2.30)$$

To summarize, the coefficient of the site tensor (2.14) is given by

$$T_{I_1 I_2 I_3 I_4; j_1 k_1 j_2 k_2 i_3 k_3 i_4 k_4; mn}^{(\alpha)} = \sum_{i_1, i_2, j_3, j_4} S_{I_1 I_2 I_3 I_4; i_1 i_2 i_3 i_4}^{(\alpha)} P_{j_1 j_2 j_3 j_4}^{(\alpha)} L_{i_2 j_3 k_2 k_3 m} L_{j_4 i_1 k_4 k_1 n} . \quad (2.31)$$

In the above expression, the indices with subscripts 1, 2, 3, and 4 are associated with the legs pointing in the direction $+\hat{1}$, $+\hat{2}$, $-\hat{1}$ and $-\hat{2}$, respectively, whereas m and n are associated with $\varphi_{x,2}$ and $\varphi_{x,1}$, respectively. The schematic representation of the site tensor is given in Fig. 1-d).

3 The procedures of the TRG

In this section, we describe how we perform the procedures of the TRG method using the initial tensor derived in the previous section. In particular, we discuss how we compress the initial tensor efficiently by inserting isometries and explain how we perform coarse-graining in the flavor space.

3.1 Compressing the initial tensor

As one can see from the expression (2.31), the initial tensor for lattice gauge theories has typically a large dimension due to the existence of many legs. It is therefore important to compress its size first before we perform the coarse-graining procedure. Here we use the compressing procedure based on the higher-order SVD, which is frequently used in HOTRG-type algorithms [50, 21] (See also Appendix B.1.).

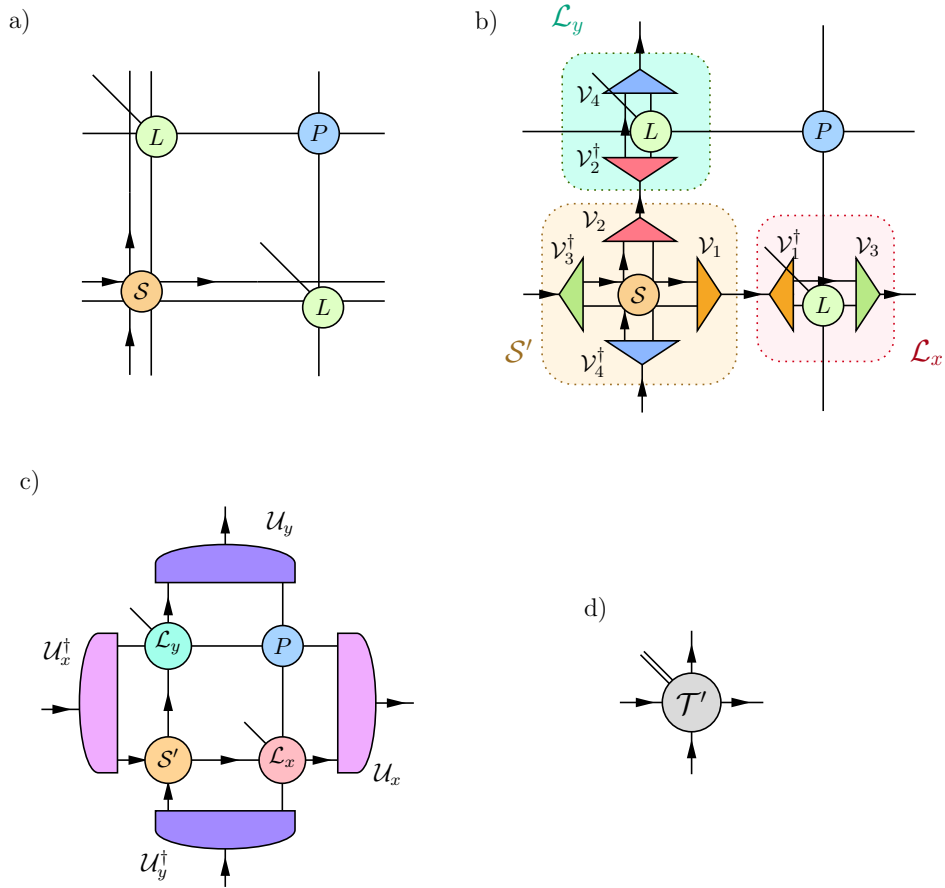


Figure 2: The schematic representation of the initial tensor compression. a) The original tensor. b) Four sets of isometries are inserted between L 's and S . c) Another set of isometries is applied to compress the whole tensor. d) The compressed initial tensor. The tensor \mathcal{V}_a in the diagram above is the isometry with the fastest-falling singular value between \mathcal{V}_{+a} and \mathcal{V}_{-a} . Similarly, U_μ is the isometry with the fastest-falling singular value between $U_{+\mu}$ and $U_{-\mu}$.

The first step of the compressing procedure is to “squeeze” the legs of the \mathcal{S} tensor (ζ_a, i_a) into a smaller leg ξ_a using the hybrid isometries that merge a fermionic leg and a bosonic leg into one fermionic leg as

$$\mathcal{S}_{\xi_1 \xi_2 \bar{\xi}_3 \bar{\xi}_4}^{(\alpha')} = \int_{\{\bar{\zeta}_\nu \zeta_\nu\}} \sum_{\{i_\nu\}} (\mathcal{V}_4)_{(\bar{\xi}_4)(\zeta_4 i_4)}^\dagger (\mathcal{V}_3)_{(\bar{\xi}_3)(\zeta_3 i_3)}^\dagger \mathcal{S}_{\zeta_1 \zeta_2 \bar{\zeta}_3 \bar{\zeta}_4; i_1 i_2 i_3 i_4}^{(\alpha)} (\mathcal{V}_1)_{(\bar{\zeta}_1 i_1)(\xi_1)} (\mathcal{V}_2)_{(\bar{\zeta}_2 i_2)(\xi_2)} , \quad (3.1)$$

where the Hermitian conjugate is defined in (A.25) and the contraction $\int_{\bar{\zeta}_\nu \zeta_\nu}$ of the bond $(\zeta_\nu, \bar{\zeta}_\nu)$ is defined in (A.20). Here we have inserted four isometries; namely \mathcal{V}_1 and \mathcal{V}_2 are inserted in the inner links between \mathcal{S} and the Kronecker delta nodes L , whereas \mathcal{V}_3 and \mathcal{V}_4 are inserted in the outer links (See Fig. 2-b). In order to obtain these isometries, we first define the tensors (repeating indices are not summed; See Fig. 3.)

$$(\mathcal{Q}_1)_{\zeta_1 \zeta_2 \bar{\zeta}_3 \bar{\zeta}_4; i_1 i_2 i_3 i_4; m} = \mathcal{S}_{\zeta_1 \zeta_2 \bar{\zeta}_3 \bar{\zeta}_4; i_1 i_2 i_3 i_4}^{(\alpha)} \delta_{i_3 m} , \quad (3.2)$$

$$(\mathcal{Q}_2)_{\zeta_1 \zeta_2 \bar{\zeta}_3 \bar{\zeta}_4; i_1 i_2 i_3 i_4; m} = \mathcal{S}_{\zeta_1 \zeta_2 \bar{\zeta}_3 \bar{\zeta}_4; i_1 i_2 i_3 i_4}^{(\alpha)} \delta_{i_4 m} , \quad (3.3)$$

$$(\mathcal{Q}_3)_{\zeta_1 \zeta_2 \bar{\zeta}_3 \bar{\zeta}_4; i_1 i_2 i_3 i_4; m} = \mathcal{S}_{\zeta_1 \zeta_2 \bar{\zeta}_3 \bar{\zeta}_4; i_1 i_2 i_3 i_4}^{(\alpha)} \delta_{i_1 m} , \quad (3.4)$$

$$(\mathcal{Q}_4)_{\zeta_1 \zeta_2 \bar{\zeta}_3 \bar{\zeta}_4; i_1 i_2 i_3 i_4; m} = \mathcal{S}_{\zeta_1 \zeta_2 \bar{\zeta}_3 \bar{\zeta}_4; i_1 i_2 i_3 i_4}^{(\alpha)} \delta_{i_2 m} \quad (3.5)$$

and construct the Grassmann Hermitian matrices

$$(\mathcal{M}_{+1})_{(\bar{\zeta}_1 i_1)(\zeta'_1 i'_1)} = \sum_{i_2, i_3, i_4, m} \int_{\substack{\bar{\zeta}_2 \zeta_2, \\ \bar{\zeta}_3 \zeta_3, \\ \bar{\zeta}_4 \zeta_4}} (\mathcal{Q}_1)_{(\bar{\zeta}_1 i_1)(\bar{\zeta}_2 \zeta_3 \zeta_4 i_2 i_3 i_4 m)}^\dagger (\mathcal{Q}_1)_{(\zeta_2 \bar{\zeta}_3 \bar{\zeta}_4 i_2 i_3 i_4 m)(\zeta'_1 i'_1)} , \quad (3.6)$$

$$(\mathcal{M}_{-1})_{(\bar{\zeta}_3 i_3)(\zeta'_3 i'_3)} = \sum_{i_1, i_2, i_4, m} \int_{\substack{\bar{\zeta}_1 \zeta_1, \\ \bar{\zeta}_2 \zeta_2, \\ \bar{\zeta}_4 \zeta_4}} (\mathcal{Q}_1)_{(\bar{\zeta}_3 i_3)(\zeta_1 \zeta_2 \bar{\zeta}_4 i_1 i_2 i_4 m)}^\dagger (\mathcal{Q}_1)_{(\bar{\zeta}_1 \bar{\zeta}_2 \zeta_4 i_1 i_2 i_4 m)(\zeta'_3 i'_3)} , \quad (3.7)$$

$$(\mathcal{M}_{+2})_{(\bar{\zeta}_2 i_2)(\zeta'_2 i'_2)} = \sum_{i_1, i_3, i_4, m} \int_{\substack{\bar{\zeta}_1 \zeta_1, \\ \bar{\zeta}_3 \zeta_3, \\ \bar{\zeta}_4 \zeta_4}} (\mathcal{Q}_2)_{(\bar{\zeta}_2 i_2)(\bar{\zeta}_1 \zeta_3 \zeta_4 i_1 i_3 i_4 m)}^\dagger (\mathcal{Q}_2)_{(\zeta_1 \bar{\zeta}_3 \bar{\zeta}_4 i_1 i_3 i_4 m)(\zeta'_2 i'_2)} , \quad (3.8)$$

$$(\mathcal{M}_{-2})_{(\bar{\zeta}_4 i_4)(\zeta'_4 i'_4)} = \sum_{i_1, i_2, i_3, m} \int_{\substack{\bar{\zeta}_1 \zeta_1, \\ \bar{\zeta}_2 \zeta_2, \\ \bar{\zeta}_3 \zeta_3}} (\mathcal{Q}_2)_{(\bar{\zeta}_4 i_4)(\zeta_1 \zeta_2 \bar{\zeta}_3 i_1 i_2 i_3 m)}^\dagger (\mathcal{Q}_2)_{(\bar{\zeta}_1 \bar{\zeta}_2 \zeta_3 i_1 i_2 i_3 m)(\zeta'_4 i'_4)} , \quad (3.9)$$

$$(\mathcal{M}_{+3})_{(\bar{\zeta}_1 i_1)(\zeta'_1 i'_1)} = \sum_{i_2, i_3, i_4, m} \int_{\substack{\bar{\zeta}_2 \zeta_2, \\ \bar{\zeta}_3 \zeta_3, \\ \bar{\zeta}_4 \zeta_4}} (\mathcal{Q}_3)_{(\bar{\zeta}_1 i_1)(\bar{\zeta}_2 \zeta_3 \zeta_4 i_2 i_3 i_4 m)}^\dagger (\mathcal{Q}_3)_{(\zeta_2 \bar{\zeta}_3 \bar{\zeta}_4 i_2 i_3 i_4 m)(\zeta'_1 i'_1)} , \quad (3.10)$$

$$(\mathcal{M}_{-3})_{(\bar{\zeta}_3 i_3)(\zeta'_3 i'_3)} = \sum_{i_1, i_2, i_4, m} \int_{\substack{\bar{\zeta}_1 \zeta_1, \\ \bar{\zeta}_2 \zeta_2, \\ \bar{\zeta}_4 \zeta_4}} (\mathcal{Q}_3)_{(\bar{\zeta}_3 i_3)(\zeta_1 \zeta_2 \bar{\zeta}_4 i_1 i_2 i_4 m)}^\dagger (\mathcal{Q}_3)_{(\bar{\zeta}_1 \bar{\zeta}_2 \zeta_4 i_1 i_2 i_4 m)(\zeta'_3 i'_3)} , \quad (3.11)$$

$$(\mathcal{M}_{+4})_{(\bar{\zeta}_2 i_2)(\zeta'_2 i'_2)} = \sum_{i_1, i_3, i_4, m} \int_{\substack{\bar{\zeta}_1 \zeta_1, \\ \bar{\zeta}_3 \zeta_3, \\ \bar{\zeta}_4 \zeta_4}} (\mathcal{Q}_4)_{(\bar{\zeta}_2 i_2)(\bar{\zeta}_1 \zeta_3 \zeta_4 i_1 i_3 i_4 m)}^\dagger (\mathcal{Q}_4)_{(\zeta_1 \bar{\zeta}_3 \bar{\zeta}_4 i_1 i_3 i_4 m)(\zeta'_2 i'_2)} , \quad (3.12)$$

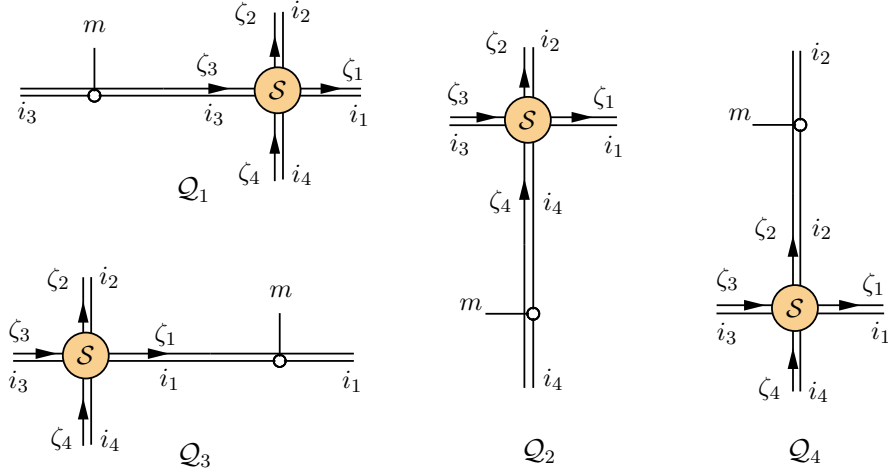


Figure 3: The \mathcal{Q} tensors used in the computation of the four isometries. \mathcal{Q}_1 and \mathcal{Q}_2 are used to compute the inner isometries, while \mathcal{Q}_3 and \mathcal{Q}_4 are used to compute the outer isometries in Fig. 2-b). The five-legged L -tensor in Fig. 2-a) are replaced by the three-legged nodes since both of these diagrams result in the same M matrices (3.6)-(3.13). Note that the position of \mathcal{S} and the Kronecker delta nodes are swapped in the inner and outer cases for a given axis.

$$(\mathcal{M}_{-4})_{(\bar{\zeta}_4 i_4)(\zeta'_4 i'_4)} = \sum_{i_1, i_2, i_3, m} \int_{\substack{\bar{\zeta}_1 \zeta_1, \\ \zeta_2 \zeta_2, \\ \zeta_3 \zeta_3}} (\mathcal{Q}_4)_{(\bar{\zeta}_4 i_4)(\zeta_1 \zeta_2 \zeta_3 i_1 i_2 i_3 m)} (\mathcal{Q}_4)^\dagger_{(\bar{\zeta}_1 \bar{\zeta}_2 \zeta_3 i_1 i_2 i_3 m)(\zeta'_4 i'_4)} , \quad (3.13)$$

where the indices in the parenthesis are combined into a single index with the prescription (A.17)-(A.18), and the Hermitian conjugate of a two-legged Grassmann tensor is defined in (A.25). Note also that the coefficient tensor with reordered indices should have appropriate sign factors due to the permutation of Grassmann-odd variables.

Then we diagonalize the Hermitian matrices $\mathcal{M}_{\pm a}$, which gives the unitary matrices $\mathcal{V}_{\pm a}$. By comparing the singular value spectra of \mathcal{M}_{+a} and \mathcal{M}_{-a} , we define the isometry in (3.1) by the unitary matrix $\mathcal{V}_{\pm a}$ that corresponds to the one with the fastest falling spectrum.

Corresponding to (3.1), we have to attach the same isometries on L as

$$(\mathcal{L}_x^{(\alpha)})_{\bar{\xi}_1 \xi_3 j_4 k_4 n} = \sum_{i_1, k_1} \int_{\bar{\zeta}_x \zeta_x} (\mathcal{V}_1)^\dagger_{(\bar{\xi}_1)(\zeta_x i_1)} (\mathcal{V}_3)_{(\bar{\zeta}_x k_1)(\xi_3)} L_{j_4 i_1 k_4 k_1 n} \quad (3.14)$$

$$= \int_{\bar{\zeta}_x \zeta_x} (\mathcal{V}_1)^\dagger_{(\bar{\xi}_1)(\zeta_x n)} (\mathcal{V}_3)_{(\bar{\zeta}_x n)(\xi_3)} \delta_{j_4 n} \delta_{k_4 n} , \quad (3.15)$$

$$(\mathcal{L}_y^{(\alpha)})_{\bar{\xi}_2 \xi_4 j_3 k_3 m} = \sum_{i_2, k_2} \int_{\bar{\zeta}_y \zeta_y} (\mathcal{V}_2)^\dagger_{(\bar{\xi}_2)(\zeta_y i_2)} (\mathcal{V}_4)_{(\bar{\zeta}_y k_2)(\xi_4)} L_{i_2 j_3 k_2 k_3 m} \quad (3.16)$$

$$= \int_{\bar{\zeta}_y \zeta_y} (\mathcal{V}_2)_{(\bar{\xi}_2)(\zeta_y m)}^\dagger (\mathcal{V}_4)_{(\bar{\zeta}_y m)(\xi_4)} \delta_{j_3 m} \delta_{k_3 m} . \quad (3.17)$$

Despite having many indices, these tensors are actually sparse due to the Kronecker deltas, which makes it more efficient to use sparse array algorithms to perform the calculation. The schematic representation of the construction of \mathcal{S}' , \mathcal{L}_x and \mathcal{L}_y is given in Fig. 2-b.

Now that we have rewritten the site tensors in terms of four sparse subtensors, we can proceed to perform the final compression, which further reduces the size of the site tensor. This can be done in exactly the same way as we have done in compressing \mathcal{S} . We first contract all the tensors together as

$$\tilde{\mathcal{T}}_{\xi_1 \xi_2 \bar{\xi}_3 \bar{\xi}_4; i_1 i_2 i_3 i_4; mn}^{(\alpha)} = \int_{\bar{\xi}_x \xi_x, \bar{\xi}_y \xi_y} P_{i_1 i_2 i_3 i_4}^{(\alpha)} \mathcal{S}_{\xi_x \xi_y \bar{\xi}_3 \bar{\xi}_4}^{(\alpha')} (\mathcal{L}_x^{(\alpha)})_{\bar{\xi}_x \xi_1 i_4 i_4 n} (\mathcal{L}_y^{(\alpha)})_{\bar{\xi}_y \xi_2 i_3 i_3 m} , \quad (3.18)$$

where the repeated indices i_3 and i_4 are not summed over. Then we construct the Hermitian matrices

$$(\tilde{\mathcal{M}}_{+x})_{(\bar{\xi}_1 i_1)(\xi'_1 i'_1)} = \sum_{i_2, i_3, i_4, m, n} \int_{\bar{\xi}_2 \xi_2, \bar{\xi}_3 \xi_3, \bar{\xi}_4 \xi_4} \tilde{\mathcal{T}}_{(\bar{\xi}_1 i_1)(\bar{\xi}_2 \xi_3 \xi_4 i_2 i_3 i_4 mn)}^{(\alpha)\dagger} \tilde{\mathcal{T}}_{(\xi_2 \bar{\xi}_3 \bar{\xi}_4 i_2 i_3 i_4 mn)(\xi'_1 i'_1)}^{(\alpha)} , \quad (3.19)$$

$$(\tilde{\mathcal{M}}_{-x})_{(\bar{\xi}_3 i_3)(\xi'_3 i'_3)} = \sum_{i_1, i_2, i_4, m, n} \int_{\bar{\xi}_1 \xi_1, \bar{\xi}_2 \xi_2, \bar{\xi}_4 \xi_4} \tilde{\mathcal{T}}_{(\bar{\xi}_3 i_3)(\xi_1 \xi_2 \bar{\xi}_4 i_1 i_2 i_4 mn)}^{(\alpha)} \tilde{\mathcal{T}}_{(\bar{\xi}_1 \bar{\xi}_2 \bar{\xi}_4 i_1 i_2 i_4 mn)(\xi'_3 i'_3)}^{(\alpha)\dagger} , \quad (3.20)$$

$$(\tilde{\mathcal{M}}_{+y})_{(\bar{\xi}_2 i_2)(\xi'_2 i'_2)} = \sum_{i_1, i_3, i_4, m, n} \int_{\bar{\xi}_1 \xi_1, \bar{\xi}_3 \xi_3, \bar{\xi}_4 \xi_4} \tilde{\mathcal{T}}_{(\bar{\xi}_2 i_2)(\bar{\xi}_1 \xi_3 \xi_4 i_1 i_3 i_4 mn)}^{(\alpha)\dagger} \tilde{\mathcal{T}}_{(\xi_1 \bar{\xi}_3 \bar{\xi}_4 i_1 i_3 i_4 mn)(\xi'_2 i'_2)}^{(\alpha)} , \quad (3.21)$$

$$(\tilde{\mathcal{M}}_{-y})_{(\bar{\xi}_4 i_4)(\xi'_4 i'_4)} = \sum_{i_1, i_2, i_3, m, n} \int_{\bar{\xi}_1 \xi_1, \bar{\xi}_2 \xi_2, \bar{\xi}_3 \xi_3} \tilde{\mathcal{T}}_{(\bar{\xi}_4 i_4)(\xi_1 \xi_2 \bar{\xi}_3 i_1 i_2 i_3 mn)}^{(\alpha)} \tilde{\mathcal{T}}_{(\bar{\xi}_1 \bar{\xi}_2 \bar{\xi}_3 i_1 i_2 i_3 mn)(\xi'_4 i'_4)}^{(\alpha)\dagger} . \quad (3.22)$$

By diagonalizing these matrices, we obtain the hybrid isometries $(\mathcal{U}_{\pm\mu})_{\bar{\xi}_i; \phi}$ that further combine the bosonic and fermionic indices together. Just like $(\mathcal{V}_{\pm a})_{\bar{\zeta}_j; \xi}$, the combined index ϕ is also truncated with the bond dimension χ_c . Thus the final compressed tensor becomes (See Fig. 2-c and -d.)

$$\mathcal{T}_{\phi_1 \phi_2 \bar{\phi}_3 \bar{\phi}_4; mn}^{(\alpha')} = \sum_{IJKL} T_{IJKL; mn}^{(\alpha')} \phi_1^I \phi_2^J \bar{\phi}_3^{\bar{K}} \bar{\phi}_4^{\bar{L}} \quad (3.23)$$

$$= \int_{\{\bar{\xi}_\nu \xi_\nu\}} \sum_{\{i_\nu\}} (\mathcal{U}_y)_{(\bar{\phi}_4)(\xi_4 i_4)}^\dagger (\mathcal{U}_x)_{(\bar{\phi}_3)(\xi_3 i_3)}^\dagger \tilde{\mathcal{T}}_{\xi_1 \xi_2 \bar{\xi}_3 \bar{\xi}_4; i_1 i_2 i_3 i_4; mn}^{(\alpha)} (\mathcal{U}_x)_{(\bar{\xi}_1 i_1)(\phi_1)} (\mathcal{U}_y)_{(\bar{\xi}_2 i_2)(\phi_2)} . \quad (3.24)$$

Here ζ 's are the four legs pointing in the 2D space, while m and n are the bosonic legs joining different flavor layers.

3.2 Some comments on the computational cost

In this subsection, we make some comments on the computational cost. The most computationally expensive parts of the process are the contraction of $\mathcal{M}_{\pm a}$ (3.6)-(3.13) and $\tilde{\mathcal{M}}_{\pm a}$

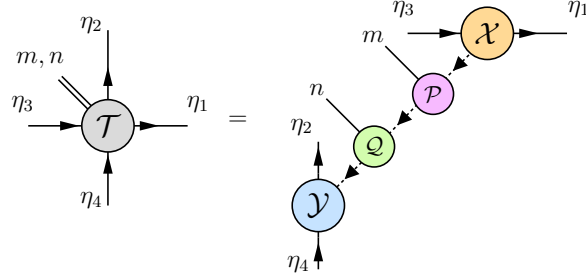


Figure 4: The decomposition of the site tensor in the modified HOTRG.

(3.19)-(3.22), which contain 11 and 12 loops, respectively. However, the number of loops in the computation of $\mathcal{M}_{\pm a}$ can be reduced since the index m is always the same as one of the other indices due to the Kronecker delta, which can effectively reduce the depth to 10 loops. In terms of complexity, the cost of the computation of $\mathcal{M}_{\pm a}$ and $\tilde{\mathcal{M}}_{\pm a}$ are $16^5 K^5$ and $D_\xi^5 K^7$, respectively, where D_ξ is the bond dimension of the fermionic legs ξ .

At the technical level, we can do a few more things to further reduce the computational cost. First, we implement another compression on the fermionic legs of the original \mathcal{S} tensor (2.27) to reduce the bond dimension of the leg ζ_a , which is of dimension $D_\zeta = 16$. In addition, we improve the speed of compression significantly by storing the tensors as sparse arrays and performing contractions with a sparse matrix-based algorithm [51].

3.3 The coarse-graining procedure

In order to perform the coarse-graining procedure in the flavor direction, we implement a modified version of HOTRG. Note first that the site tensor $\mathcal{T}'_{\eta_1 \eta_2 \bar{\eta}_3 \bar{\eta}_4; mn}$ has six indices. Four of them are the fermionic indices in the 2D space directions, while m and n are the indices for the gauge link variables. Since the site tensors in the flavor direction are connected with the Kronecker deltas, the bosonic bond degrees of freedom are maximally entangled in the flavor direction, which implies that we cannot insert isometries to compress these bonds further. For this reason, we have to perform the coarse-graining procedure in the flavor direction before the coarse-graining in the two-dimensional space.

Since the size of the compressed initial tensor (3.23) grows like K^2 with K being the bond dimension of the bosonic legs, the coarse-graining can become costly with the traditional HOTRG algorithm [21] as we increase K . (See Appendix B for a review of the HOTRG and related methods.) We therefore modify the HOTRG method by first performing the decomposition such that we separate the legs into three groups based on their axes as

$$\mathcal{T}'_{\eta_1 \eta_2 \bar{\eta}_3 \bar{\eta}_4; mn}^{(\alpha)} = \int_{\bar{\zeta}\zeta, \bar{\phi}\phi, \bar{\xi}\xi} \mathcal{X}_{\eta_1 \bar{\eta}_3 \zeta}^{(\alpha)} \mathcal{P}_{\bar{\zeta}\phi; m}^{(\alpha)} \mathcal{Q}_{\bar{\phi}\xi; n}^{(\alpha)} \mathcal{Y}_{\bar{\xi}\eta_2 \bar{\eta}_4}^{(\alpha)}, \quad (3.25)$$

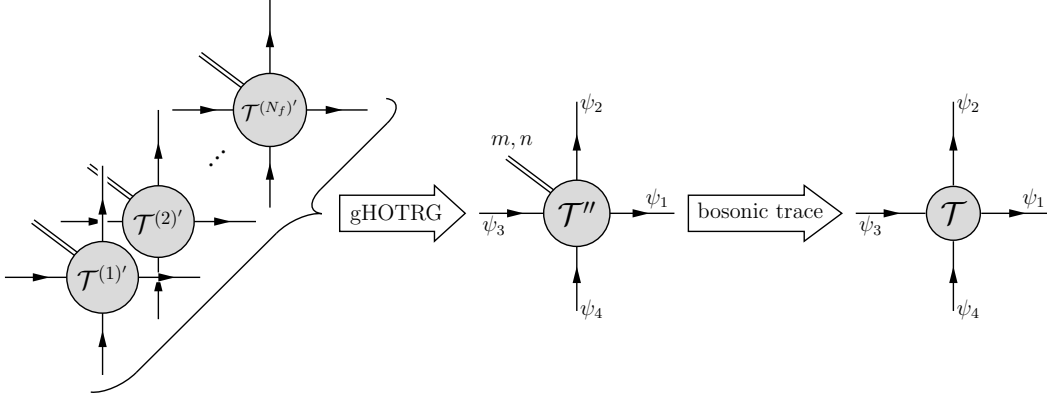


Figure 5: The summary of the flavor coarse-graining procedure.

where the legs along the x axis are in the \mathcal{X} tensor, the legs along the y axis are in the \mathcal{Y} tensor, and the legs along the flavor axis are in the \mathcal{P} and \mathcal{Q} tensors. With this decomposition, the isometries along the x and y axis are computed using the tensor \mathcal{X} and \mathcal{Y} , respectively.

In order to obtain the partition function, we first perform coarse-graining procedure in the z (flavor) direction using the Grassmann higher-order TRG (gHOTRG) algorithm described in Appendix B.1, which gives us the N_f -flavor tensor $\mathcal{T}''_{\psi_1\psi_2\bar{\psi}_3\bar{\psi}_4;mn}$. Then we take the trace of the bosonic indices

$$\mathcal{T}_{\psi_1\psi_2\bar{\psi}_3\bar{\psi}_4} = \sum_{m,n} \mathcal{T}''_{\psi_1\psi_2\bar{\psi}_3\bar{\psi}_4;mn} , \quad (3.26)$$

which is described schematically in Fig. 5.

Next, we perform the coarse-graining in the 2D plane using the Grassmann TRG (gTRG) which is described in detail in Appendix B.2. The bond dimensions for the gHOTRG in the flavor direction is χ_f , while the bond dimension for gTRG in the 2D plane is χ_{xy} . After performing the coarse-graining procedure sufficiently many times, we take the trace of the final tensor with anti-periodic boundary conditions in the imaginary time direction to obtain the partition function as

$$Z = \sum_{I,J} T_{IJIJ} \sigma_I \sigma_J (-)^{p(I)p(J)+p(J)} , \quad (3.27)$$

where σ_I is the sign factor defined in (A.11).

All of the computations in this paper are done using a Python package `grassmanntn` [52] specialized in handling the Grassmann tensor network.

β	$\tilde{\mu}$	N_f	K	original size	compressed size	compression ratio	D_x	D_y
0.0	0.0	1	2	67108864	1024	1.53×10^{-5}	4	4
0.0	0.0	1	3	3869835264	2304	5.95×10^{-7}	4	4
0.0	0.0	1	4	68719476736	4096	5.96×10^{-8}	4	4
0.0	0.0	1	5	640000000000	6400	1.00×10^{-9}	4	4
2.0	0.0	1	2	67108864	16384	2.44×10^{-4}	8	8
2.0	0.0	2	2	67108864	16384	2.44×10^{-4}	8	8
2.0	3.0	1	2	67108864	16384	2.44×10^{-4}	8	8
2.0	3.0	2	2	67108864	16384	2.44×10^{-4}	8	8

Table 1: Summary of the initial tensor compression for various input parameters β , $\tilde{\mu}$, N_f , and K . The relative error of the compression is less than 10^{-15} for all the cases. The size of the original tensor is obtained by the formula $16^4 K^{10}$, whereas that of the compressed tensor is obtained by $(D_x D_y K)^2$. Here D_x and D_y represent the bond dimension of the legs I_1 and I_3 and the bond dimension of the legs I_2 and I_4 , respectively, of the compressed coefficient tensor $T_{I_1 I_2 I_3 I_4; mn}^{(\alpha)'}$, while K represents the bond dimension of the bosonic legs m and n .

4 Numerical results

In this section, we present our numerical results obtained by the method introduced in the previous sections. First, we perform performance tests concerning the initial tensor compression described in section 3.1 and the coarse-graining procedure in the flavor direction described in section 3.3. Then we demonstrate the usefulness of our method by investigating the chiral phase transition and the Silver Blaze phenomenon in 2D Abelian gauge theories. In what follows, we assume that all the flavors of fermions have the same charge $q_\alpha = q$, mass $\tilde{m}_\alpha = \tilde{m}$ and chemical potential $\tilde{\mu}_\alpha = \tilde{\mu}$.

4.1 Performance tests

Let us first demonstrate the efficiency of the initial tensor compression. For that, we compute $\log Z$ for various parameters and measure the errors by comparing the results obtained with and without compression. It is found that the relative error of the compression is less than 10^{-15} for all the cases if we choose the compression bond dimension $\chi_c = 64$. The efficiency of the compression for this choice is summarized in Table 1. It is clear that our compression scheme is efficient, in particular for large K , where the original tensor can easily become too large to be handled by the currently available computers.

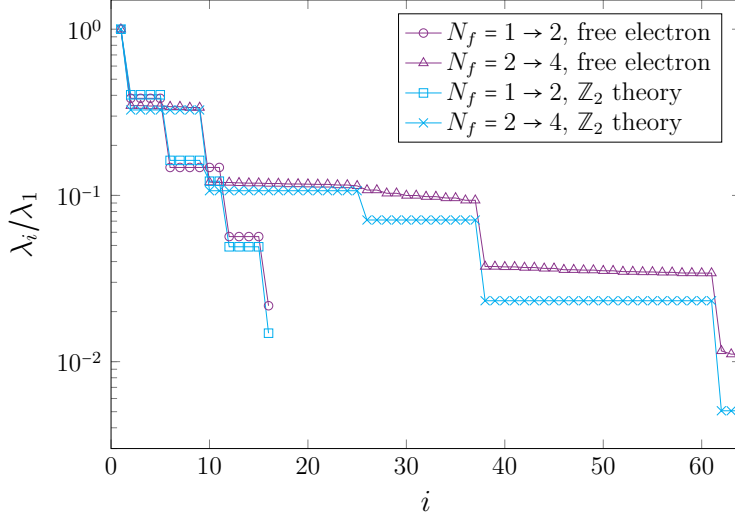


Figure 6: The singular value spectrum associated with the HOTRG isometry truncation in the free electron gas model and the \mathbb{Z}_2 gauge theory. Here we show only the spectra of the x -axis truncation, which is identical to that of the y -axis truncation.

Next, we discuss the performance of coarse-graining in the flavor direction. Here we perform the gHOTRG up to $N_f = 4$ for the free electron gas model ($K = 1$) and the \mathbb{Z}_2 gauge theory with $\beta = 0$, $q = 1$, $\tilde{m} = 1$ and $\tilde{\mu} = 0$. In Fig. 6, we plot the singular value spectra associated with the SVD when the isometries (\mathcal{U}_x and \mathcal{U}_y in (B.14) and (B.15)) are used during the step $N_f = 1 \rightarrow 2$ and $2 \rightarrow 4$ with $\chi_f = 64$. One can see that the tail of the singular value spectrum grows quickly with N_f , which indicates that fermions from different layers have strong degeneracy. Note that introducing gauge interaction makes the singular value spectrum decays faster. For the calculations in the subsequent subsections, we use $\chi_f = 64$ for $N_f = 2$ and $\chi_f = 32$ for $N_f = 4$ for the flavor coarse-graining, and $\chi_{xy} = 64$ for the two-dimensional coarse-graining.

4.2 The chiral phase transition

In order to demonstrate the usefulness of our method, we first apply it to the chiral phase transition in two-flavor \mathbb{Z}_2 , \mathbb{Z}_4 , and $U(1)$ gauge theories. Let us define the hopping parameter by

$$\kappa = \frac{1}{2\tilde{m} + 4}. \quad (4.1)$$

Although the chiral symmetry is broken explicitly by the Wilson term in (2.3), it is expected to be restored at some critical hopping parameter κ_c . We can easily identify κ_c in the TRG

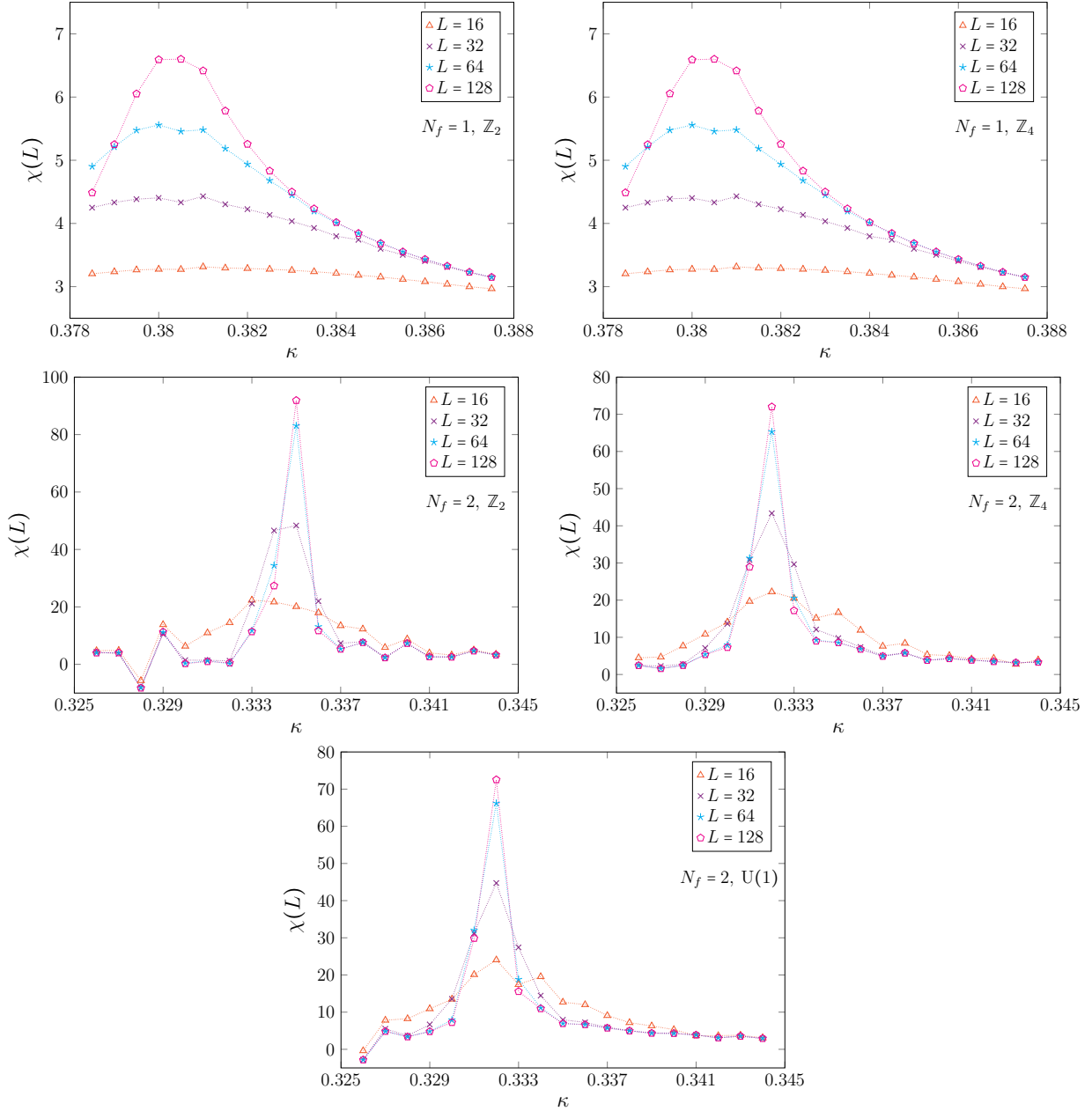


Figure 7: Chiral susceptibility is plotted as a function of κ at $\beta = 0$ for different gauge theories and N_f (labeled in each plot) with lattice volume up to $V = 128^2$. The dotted lines are shown to guide the eyes. The critical hopping parameter κ_c can be identified as the location of the peak in the infinite volume limit. Note that the plots for $N_f = 1$ are almost identical for the \mathbb{Z}_2 and \mathbb{Z}_4 cases.

Gauge group	Algorithm	κ_c
\mathbb{Z}_2	gTRG	0.335(1)
\mathbb{Z}_4	gTRG	0.332(1)
U(1)	gTRG	0.332(1)
U(1)	Monte Carlo [48]	0.3296983759

Table 2: The critical hopping parameter for various gauge theories with $N_f = 2$ at $\beta = 0$. Our U(1) result is computed with the 4-nodes Gauss-Legendre quadrature.

method by the location of the peak of chiral susceptibility

$$\chi(L) = \frac{1}{V} \frac{\partial^2}{\partial \tilde{m}^2} \log Z \quad (4.2)$$

given as a function of the hopping parameter κ , where the derivatives can be taken numerically. The peak of the chiral susceptibility exhibits a critical behavior in the large volume limit as demonstrated in Ref. [27] with $N_f = 1$. In Fig. 7. we observe similar behavior in various gauge theories with $N_f = 1$ and 2 at $\beta = 0$, where we have used $\chi_f = \chi_{xy} = 64$. For the U(1) case, we use the 4-nodes Gauss-Legendre quadrature to discretize the group integral.

In the large- K limit, \mathbb{Z}_K gauge theory converges to the U(1) gauge theory. For $N_f = 1$, the critical hopping parameter $\kappa_c = 0.3806(1)$ obtained by our method in both \mathbb{Z}_2 and \mathbb{Z}_4 theories is consistent with the result $\kappa_c = 0.380665(59)$ obtained for the U(1) $\simeq \mathbb{Z}_\infty$ theory in Ref. [27], which indicates that the convergence occurs already at $K = 2$ for $\beta = 0$. For $N_f = 2$, we obtain κ_c for the \mathbb{Z}_2 , \mathbb{Z}_4 , and U(1) theories at $\beta = 0$ and compare with the Monte Carlo results for the U(1) theory [48] in table 2.

4.3 Silver Blaze phenomenon at finite density

Next we apply our method to the finite density case with multiple flavors. In particular, it is expected that physical observables in the thermodynamic limit and at zero temperature are independent of the chemical potential up to some threshold due to the gapped spectrum in the confined phase. This is known as the Silver Blaze phenomenon [53], which is difficult to reproduce by Monte Carlo methods due to the sign problem. We investigate this phenomenon by our method to demonstrate that the sign problem is indeed solved.

Here we consider the \mathbb{Z}_2 gauge theory and the free electron model with $\beta = 1$, $q = 1$, $\tilde{m} = 1$. We calculate the pressure and the number density

$$P(\tilde{\mu}) = \frac{1}{V} \log Z , \quad (4.3)$$

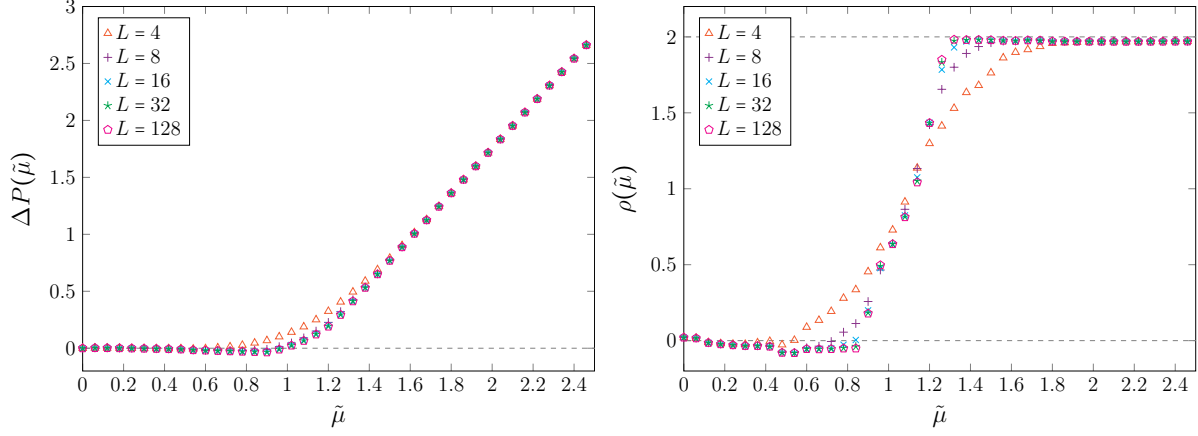


Figure 8: Differential pressure $\Delta P(\tilde{\mu})$ and number density $\rho(\tilde{\mu})$ of the \mathbb{Z}_2 gauge theory with $N_f = 2$ at various volume $V = L \times L$. The small non-monotonicity may be attributed to the finite truncation effect.

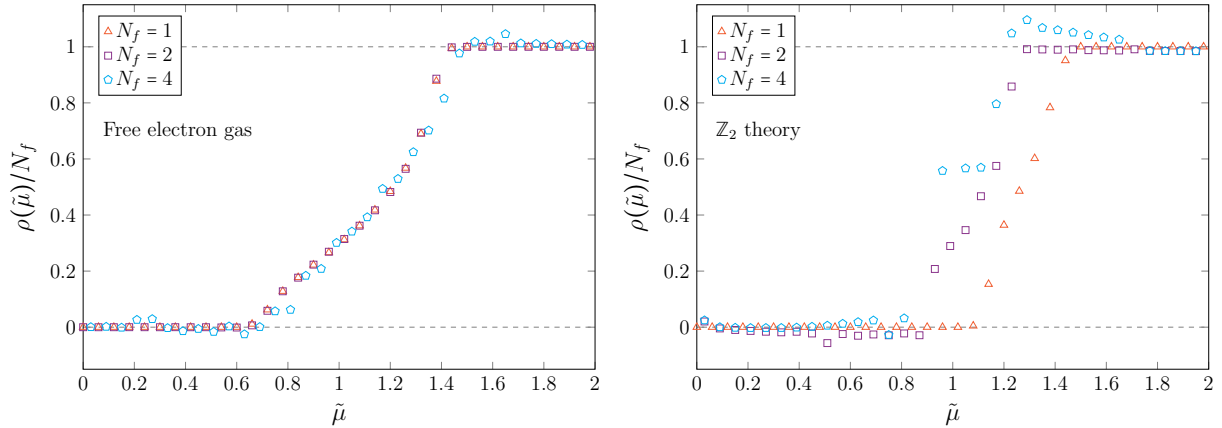


Figure 9: $\rho(\tilde{\mu})/N_f$ is plotted against $\tilde{\mu}$ for $V = 128 \times 128$ in the free electron model and the \mathbb{Z}_2 gauge theory with $N_f = 1, 2,$ and 4 . The non-monotonicity may be attributed to the truncation effect, which becomes more significant for larger N_f .

$$\rho(\tilde{\mu}) = \frac{\partial P}{\partial \tilde{\mu}}, \quad (4.4)$$

where the derivative in (4.4) is taken numerically.

In Fig. 8 we plot the differential pressure $\Delta P(\tilde{\mu}) = P(\tilde{\mu}) - P(0)$ and the number density $\rho(\tilde{\mu})$ against $\tilde{\mu}$ up to the volume $V = 128 \times 128$ in the \mathbb{Z}_2 gauge theory with $N_f = 2$. We observe a clear Silver Blaze phenomenon for $\tilde{\mu} \lesssim 0.8$. We also find that the number density saturates to the value $\rho = 2$ for $\tilde{\mu} > 1.4$ as expected from the number of degrees of freedom at each lattice site.

In Fig. 9 we plot $\rho(\tilde{\mu})/N_f$ against $\tilde{\mu}$ in the free electron model and the \mathbb{Z}_2 gauge theory with $N_f = 1, 2$, and 4. The number density saturates to the value $\rho = N_f$ for all cases. Note also that in the free electron gas model, $\rho(\tilde{\mu})/N_f$ are expected to be the same for all N_f , which is not the case in the \mathbb{Z}_2 gauge theory due to interactions.

5 Summary

In this paper, we have proposed a new technique to incorporate multiple flavors in the TRG method for lattice gauge theories. The problem of the initial tensor, which grows in size exponentially with the number of flavors N_f , has been overcome by separating the initial tensor into N_f layers with replicas of the gauge field for each layer, which are identified later. This effectively makes the system one dimension higher due to the flavor direction. Consequently, the tensor can still be large, in particular, due to the gauge field legs in the extra dimension. In order to overcome this problem, we use a compression scheme, which proceeds in two steps by truncating first the subtensors and then the whole tensor. We have shown that this enables us to compress the size of the initial tensor by many orders of magnitude without sacrificing the accuracy. Notably, the compression is found to be more effective for larger K in \mathbb{Z}_K gauge theories, where the original tensor can be too large to perform any calculation with currently available computers.

As another important performance test, we have studied the singular value spectrum of the flavor coarse-graining procedure and find that introducing gauge interaction makes the spectrum decays faster. In order to demonstrate the usefulness of our method, we have investigated the chiral phase transition in two-dimensional Abelian gauge theories with $N_f = 2$ by computing the critical value of the hopping parameter, which turns out to be consistent with the known value obtained by the Monte Carlo method. We have also applied our method to the case of finite density with $N_f = 1, 2$, and 4 in the \mathbb{Z}_2 gauge theory. In particular, we were able to observe the Silver Blaze phenomenon, which is difficult to reproduce by Monte Carlo methods due to the sign problem.

We consider that our new technique will make the TRG method applicable to many interesting gauge theories with multiple flavors that have not been explored yet. Since the main idea can be generalized to the non-Abelian case, we hope that it will be useful also in investigating QCD, where two (or three) flavors of light quarks have to be incorporated. We also expect that, by implementing better renormalization schemes such as the bond-weighting methods [20, 54] or stochastic sampling approach [55, 56, 57], the systematic error from bond truncation can be reduced. Last but not the least, we expect that our technique is useful in applying the TRG method to the domain-wall formalism for chiral fermions, where the extra dimension can be regarded as the flavor direction in our method. In that case, we need to introduce local interactions in the flavor direction as described in Appendix C. If such interactions make the singular-value spectrum in the flavor direction decay faster, one can go to larger N_f , which is crucial in the domain-wall formalism. We hope to report on this in the future publication.

Acknowledgments

We would like to thank Akira Matsumoto for valuable discussions and Abhabongse Jantong for valuable advice in code development and optimization. A. Y. and K. O. are supported by a Grant-in-Aid for Transformative Research Areas “The Natural Laws of Extreme Universe—A New Paradigm for Spacetime and Matter from Quantum Information” (KAKENHI Grant No. JP21H05191) from JSPS of Japan.

A Grassmann tensor network

In this section, we provide a formulation of the Grassmann tensor network, where we explore the Grassmann tensor and its properties in more detail than in the original paper [28]. In particular, we propose a new format for the coefficient tensor that has an intuitive connection with the non-Grassmann linear algebra.

In general, one can expand any function of Grassmann variables as a polynomial

$$\mathcal{T}(\theta_1, \theta_2, \dots, \theta_n) \equiv \mathcal{T}_{\theta_1 \theta_2 \dots \theta_n} = \sum_{i_1 i_2 \dots i_n \in \{0,1\}} T_{i_1 i_2 \dots i_n} \theta_1^{i_1} \theta_2^{i_2} \dots \theta_n^{i_n}, \quad (\text{A.1})$$

where the complex-valued coefficient $T_{i_1 i_2 \dots i_n}$ shall be referred to as the *coefficient tensor*. Multiple Grassmann numbers can be grouped into a single multi-component variable, for instance, as

$$\psi^I \equiv \theta_1^{i_1} \dots \theta_m^{i_m}, \quad (\text{A.2})$$

where $I = (i_1, \dots, i_m)$. Hereafter, we reserve the symbol θ for a one-component Grassmann number and use other Greek letters for multi-component Grassmann numbers. In practice, the composite index I must be encoded as an integer with some binary encoder $f(i_1, \dots, i_m) \in \mathbb{Z}$. Physical quantities are independent of the encoding function, but the calculation can be made easier if it is chosen appropriately. Two useful ones are the ‘‘canonical’’ and the ‘‘parity-preserving’’ [28] encoders defined, respectively, by

$$f_{\text{canonical}}(i_1, \dots, i_n) = \sum_{k=1}^n 2^{k-1} i_k, \quad (\text{A.3})$$

$$f_{\text{parity-preserving}}(i_1, \dots, i_n) = \begin{cases} \sum_{k=1}^n 2^{k-1} i_k & ; i_2 + \dots + i_n \text{ even} , \\ 1 - i_1 + \sum_{k=2}^n 2^{k-1} i_k & ; i_2 + \dots + i_n \text{ odd} . \end{cases} \quad (\text{A.4})$$

The canonical encoder is more intuitive and easier to join and split the indices, while the parity-preserving encoder is essential in the construction of the isometries, which is explained below. In this paper, both the composite index and its encoding are referred to by the same capital Latin letters for simplicity.

In order to combine two indices that are not adjacent, we have to rearrange these indices first so that the indices to be combined are next to each other. When the two indices are swapped, the coefficient tensor must be multiplied by a sign factor due to the anti-commuting nature of the Grassmann numbers. For example, if we swap T_{IJKL} into T'_{IKJL} , we have to multiply the relative sign factor coming from $\psi_1^J \psi_2^K = (-)^{p(J)p(K)} \psi_2^K \psi_1^J$ to the coefficient tensor as

$$T_{IJKL} = T'_{IKJL} (-)^{p(J)p(K)}, \quad (\text{A.5})$$

where $p(I) = \sum_a i_a$ is the Grassmann parity of ψ^I .

A.1 Grassmann tensors and their contraction

The contraction of the Grassmann indices is performed by the Berezin integral of the pair $(\bar{\theta}, \theta)$. For example, in the case of one component, we have the identity

$$\int d\bar{\theta} d\theta e^{-\bar{\theta}\theta} \theta^i \bar{\theta}^j = \delta_{ij}. \quad (\text{A.6})$$

Then the contraction of the two Grassmann tensors reads

$$\int d\bar{\theta} d\theta e^{-\bar{\theta}\theta} \mathcal{A}_{\bar{\theta}_1 \theta} \mathcal{B}_{\bar{\theta} \theta_2} = \sum_{i,j} \left(\sum_k A_{ik} B_{kj} \right) \bar{\theta}_1^i \theta_2^j. \quad (\text{A.7})$$

The multi-component case is slightly more complicated since, for $I = (i_1, \dots, i_n)$ and $\psi^I = \theta_1^{i_1} \dots \theta_n^{i_n}$, the contraction

$$\prod_{a=1}^n \int d\bar{\theta}_a d\theta_a e^{-\bar{\theta}_a \theta_a} \psi^I \bar{\psi}^J = \left(\prod_a \delta_{i_a, j_a} \right) \times \left(\prod_{a < b} (-)^{i_a i_b} \right), \quad (\text{A.8})$$

has the extra sign factor coming from rearranging θ_a and $\bar{\theta}_a$ for the integration. Defining

$$\int d\bar{\psi} d\psi e^{-\bar{\psi} \psi} \equiv \prod_{a=1}^n \int d\bar{\theta}_a d\theta_a e^{-\bar{\theta}_a \theta_a}, \quad (\text{A.9})$$

$$\delta_{IJ} \equiv \prod_a \delta_{i_a, j_a}, \quad (\text{A.10})$$

$$\sigma_I \equiv \prod_{a < b} (-)^{i_a i_b}, \quad (\text{A.11})$$

the contraction (A.8) can be rewritten in a compact form

$$\int d\bar{\psi} d\psi e^{-\bar{\psi} \psi} \psi^I \bar{\psi}^J = \delta_{IJ} \sigma_I, \quad (\text{A.12})$$

which is the multi-component counterpart of (A.6). The contraction rule according to the identity (A.12) is

$$\int d\bar{\eta} d\eta e^{-\bar{\eta} \eta} \mathcal{A}_{\bar{\psi}\eta} \mathcal{B}_{\bar{\eta}\phi} = \sum_{I,J} \left(\sum_K A_{IK} B_{KJ} \sigma_K \right) \bar{\psi}^I \phi^J, \quad (\text{A.13})$$

which differs slightly from the usual matrix contraction due to the extra sign factor σ_K .

It is possible to define a new format for the coefficient tensor such that the contraction can be done without the extra sign factor as

$$\mathcal{A}_{\bar{\psi}_1 \dots \bar{\psi}_m \phi_1 \dots \phi_n} = \sum_{I_1 \dots I_m J_1 \dots J_n} A_{I_1 \dots I_m J_1 \dots J_n}^{(m)} \sigma_{I_1} \dots \sigma_{I_m} \bar{\psi}_1^{I_1} \dots \bar{\psi}_m^{I_m} \phi_1^{J_1} \dots \phi_n^{J_n}, \quad (\text{A.14})$$

which we call the *matrix format*. The coefficient tensor in this format can be defined in terms of that in the standard format as

$$A_{I_1 \dots I_m J_1 \dots J_n}^{(m)} \equiv A_{I_1 \dots I_m J_1 \dots J_n} \sigma_{I_1} \dots \sigma_{I_m}. \quad (\text{A.15})$$

Namely we multiply the sign factor σ_{I_a} for every conjugated Grassmann index $\bar{\psi}_a^{I_a}$. It is straightforward to check that the coefficient matrix of the contraction (A.13) is actually the matrix product $A^{(m)} B^{(m)}$ as

$$\mathcal{C}_{\bar{\psi}\phi} = \int d\bar{\eta} d\eta e^{-\bar{\eta} \eta} \mathcal{A}_{\bar{\psi}\eta} \mathcal{B}_{\bar{\eta}\phi} = \sum_{I,J} (A^{(m)} B^{(m)})_{IJ} \bar{\psi}^I \phi^J = \sum_{I,J} C_{IJ}^{(m)} \sigma_I \bar{\psi}^I \phi^J. \quad (\text{A.16})$$

This simple contraction rule also applies to tensors of arbitrary rank if it is written in the matrix format. Note that the sign factors from the index permutation must also be applied if the contracted indices are not adjacent.

Tensor legs can be joined together with the prescription

$$\xi^K \equiv \psi_1^{I_1} \cdots \psi_m^{I_m} \bar{\phi}_1^{J_1} \cdots \bar{\phi}_n^{J_n} , \quad (\text{A.17})$$

$$\bar{\xi}^K \equiv \bar{\psi}_1^{I_1} \cdots \bar{\psi}_m^{I_m} \phi_1^{J_1} \cdots \phi_n^{J_n} \prod_{a=1}^n (-)^{p(J_a)} , \quad (\text{A.18})$$

$$\int d\bar{\xi} d\xi e^{-\bar{\xi}\xi} \equiv \int \prod_{a=1}^m \left(d\bar{\psi}_a d\psi_a e^{-\bar{\psi}_a \psi_a} \right) \prod_{b=1}^n \left(d\bar{\phi}_b d\phi_b e^{-\bar{\phi}_b \phi_b} \right) . \quad (\text{A.19})$$

It is important that the sign factor $(-)^{p(J_a)}$, where J_a is the index of the non-conjugated constituent ϕ_a , must be introduced if the joined variable is a conjugated fermion. This is to ensure that the contraction between ξ and $\bar{\xi}$ with the measure (A.19) follows the contraction rule (A.13).

Throughout this paper, we abbreviate the contraction integral by

$$\int_{\bar{\eta}\eta} \equiv \int d\bar{\eta} d\eta e^{-\bar{\eta}\eta} . \quad (\text{A.20})$$

Note that the Grassmann contraction is directional since the Grassmann variables are anti-commuting. Therefore the bond between any two Grassmann tensors should have an arrow pointing from η to $\bar{\eta}$.

A.2 Eigenvalue and singular-value decompositions

Here we introduce the concept of matrix decomposition for Grassmann tensors, which is similar to the one used in the traditional tensor network as an important part of the coarse-graining procedure. In this context, we assume that the tensor has already been reshaped (with (A.17)-(A.18)) into a matrix

$$\mathcal{M}_{\bar{\psi}\phi} = \sum_{IJ} M_{IJ}^{(m)} \sigma_I \bar{\psi}^I \phi^J . \quad (\text{A.21})$$

Let $v^{(m)\dagger}$ and $u^{(m)}$ be the left and right eigenvectors of $M^{(m)}$ with the eigenvalue λ as

$$v^{(m)\dagger} M^{(m)} = \lambda v^{(m)\dagger} , \quad M^{(m)} u^{(m)} = \lambda u^{(m)} . \quad (\text{A.22})$$

The Grassmann eigenvectors of \mathcal{M} can then be defined by

$$v_{\bar{\psi}}^{\dagger} = \sum_I v_I^{(m)*} \psi^I , \quad u_{\bar{\psi}} = \sum_I u_I^{(m)} \sigma_I \bar{\psi}^I . \quad (\text{A.23})$$

With this definition, the Grassmann version of the eigenvector equations follows nicely as

$$\int_{\bar{\psi}\psi} v_{\psi}^{\dagger} \mathcal{M}_{\bar{\psi}\phi} = \lambda v_{\phi}^{\dagger}, \quad \int_{\bar{\phi}\phi} \mathcal{M}_{\bar{\psi}\phi} u_{\bar{\phi}} = \lambda u_{\bar{\psi}}. \quad (\text{A.24})$$

Next the Hermitian conjugate of \mathcal{M} is given by

$$\mathcal{M}_{\bar{\psi}\phi}^{\dagger} = \sum_{I,J} M_{JI}^{(m)*} \sigma_I \bar{\psi}^I \phi^J. \quad (\text{A.25})$$

Note how the notion of Hermiticity, unitarity, and duality of the vector space is straightforward and intuitive when the coefficient tensor is written in the matrix format. With all of these defined, we can write the Grassmann version of the singular value decomposition (gSVD) or the eigen decomposition (gEigD) as

$$\mathcal{M}_{\bar{\psi}\phi} = \int_{\bar{\eta}\eta} \int_{\bar{\zeta}\zeta} \mathcal{U}_{\bar{\psi}\eta} \text{diag}(\lambda)_{\bar{\eta}\zeta} \mathcal{V}_{\bar{\zeta}\phi}^{\dagger}, \quad (\text{A.26})$$

where

$$\text{diag}(\lambda)_{\bar{\phi}\psi} = \sum_I \lambda_I \sigma_I \bar{\phi}^I \psi^I. \quad (\text{A.27})$$

The unitary matrices \mathcal{U} , \mathcal{V} and $\text{diag}(\lambda)$ are obtained as follows. We first obtain the coefficient matrix $M_{IJ}^{(m)}$ with the parity-preserving encoder (A.4). If \mathcal{M} is Grassmann even, $M^{(m)}$ can be diagonalized into two blocks with I, J even and odd, respectively.

$$M_{IJ}^{\text{E}} = M_{2I,2J}^{(m)}, \quad M_{IJ}^{\text{O}} = M_{2I-1,2J-1}^{(m)}. \quad (\text{A.28})$$

These two blocks are diagonalized separately and give two sets of unitary matrices ($U^{\text{E}}, V^{\text{E}}$) and ($U^{\text{O}}, V^{\text{O}}$). The full unitary matrices ($U^{(m)}, V^{(m)}$) are subsequently obtained by

$$U_{2I,2J}^{(m)} = U_{IJ}^{\text{E}}, \quad U_{2I-1,2J-1}^{(m)} = U_{IJ}^{\text{O}}, \quad (\text{A.29})$$

$$V_{2I,2J}^{(m)} = V_{IJ}^{\text{E}}, \quad V_{2I-1,2J-1}^{(m)} = V_{IJ}^{\text{O}}. \quad (\text{A.30})$$

Notice that the two matrix indices of $U^{(m)}$ and $V^{(m)}$ also have the same parity, which means that the Grassmann isometry \mathcal{U} obtained from $U^{(m)}$ is guaranteed to be Grassmann even, and so is \mathcal{V} . Because all the matrices in the decomposition are Grassmann even, all the tensors formed and decomposed during the coarse-graining procedures are also always Grassmann even, so the process is free from the global sign factor when we exchange the position of the tensors.

B Details of the coarse-graining procedures

In this section, we present the details of the coarse-graining procedures. There are actually two kinds of them used in this paper, namely the HOTRG method, which is used when we block the tensor in the z (flavor)-direction, and the TRG method, which is used in two-dimensional blocking.

B.1 Grassmann HOTRG

Let us first give a brief review of the non-Grassmann HOTRG method. The main idea is to insert a resolution of the identity on the bonds we wish to truncate. For example, given a two-dimensional tensor T_{ijkl} , where we wish to truncate the leg i , the most naive way is to perform an SVD and insert an identity $U^\dagger U$ on that leg as

$$T_{ijkl} = \sum_a U_{ia} \lambda_a V_{ajkl} = \sum_{a,b,i'} U_{ib} (U_{bi'}^\dagger U_{i'a}) \lambda_a V_{ajkl}, \quad (\text{B.1})$$

where the legs a and b are truncated. The schematic representation of this process is shown in Fig. 10-a to -c. If the legs i and k in T_{ijkl} are contracted on a periodic lattice, which means that they are pointing in the opposite direction, the isometry U_{ib} can be moved to contract with k instead as

$$\sum_{a,b,i'} U_{ib} U_{bi'}^\dagger U_{i'a} \lambda_a V_{ajkl} \rightarrow \sum_{a,i,k} U_{bi}^\dagger U_{ia} \lambda_a V_{ajkl} U_{kc} = \sum_{i,k} U_{bi}^\dagger T_{ijkl} U_{kc} \equiv T'_{bjcl}. \quad (\text{B.2})$$

Since the legs b and c are truncated, the tensor T' becomes smaller. This process is shown in Fig. 10-c to -d. Note that the isometry is not unique. If we apply the same procedure on the leg k instead, we will arrive at a different isometry. We have to choose the one that makes the singular value spectrum decay the fastest and thus allows the smallest truncation.

A more efficient but equivalent way to do this is to define a Hermitian matrix

$$M_{ii'} = \sum_{j,k,l} T_{ijkl} T_{i'jkl}^*. \quad (\text{B.3})$$

Substituting the first equality of (B.1) in (B.3), we get

$$M_{ii'} = \sum_{j,k,l,a,b} U_{ia} \lambda_a V_{ajkl} U_{i'b}^* \lambda_b V_{bjkl}^* = \sum_{j,k,l,a,b} U_{ia} \lambda_a^2 U_{ai'}^\dagger. \quad (\text{B.4})$$

In other words, we can obtain U by diagonalizing the matrix M instead of performing an SVD for a four-legged tensor T , which is much slower.

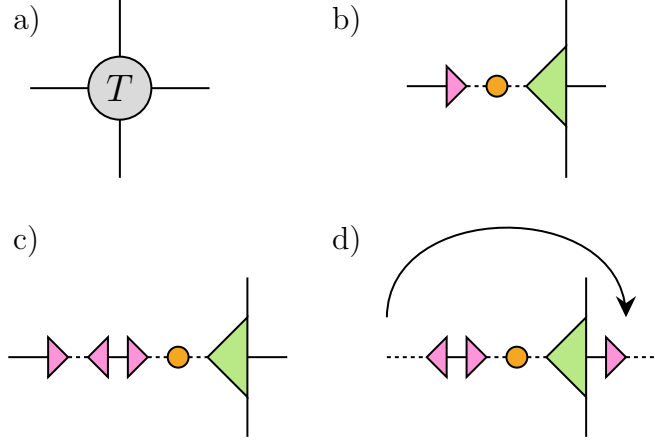


Figure 10: Schematic representation of (B.1)-(B.2). Small triangles, large triangles, and circles represent U_{ia} , V_{ajkl} and λ_a , respectively. The dashed lines represent the truncated legs. a) A four-legged tensor T_{ijkl} . b) An SVD is performed for one of the legs, i . c) A resolution of the identity $U^\dagger U$ is inserted between U and λ . d) An isometry is moved to the other side.

We can straightforwardly apply such a coarse-graining procedure to the 3-dimensional case. Given a 6-leg tensor $T_{i_1 i_2 i_3 j_1 j_2 j_3}$ with i_μ and j_μ pointing in the opposite direction, we first contract two T tensors in z direction,

$$\sum_{k_3} T_{i_1 i_2 i_3 j_1 j_2 k_3} T_{i'_1 i'_2 k_3 j'_1 j'_2 j_3} = \tilde{T}_{(i_1 i'_1)(i_2 i'_2) i_3 (j_1 j'_1)(j_2 j'_2) j_3} . \quad (\text{B.5})$$

and then attach the isometry $(U_\mu)_{(i i') \tilde{i}}$ to merge the double bond $(i_\mu i'_\mu)$ into a truncated bond \tilde{i}_μ . Note that the standard HOTRG procedure can be generalized to the Grassmann tensor network [28, 42].

For the flavor coarse-graining, however, we explain a slightly modified version of the Grassmann HOTRG to improve computational efficiency in dealing with large-size initial tensors. The key point is first to decompose the tensor of each layer into small sub-tensors and then block the legs of sub-tensors from the layers α and α' in the x and y directions separately. Namely, we perform gSVD for $\mathcal{T}^{(\alpha)}$ (See Fig. 11-a.)

$$\mathcal{T}_{\eta_1 \eta_2 \bar{\eta}_3 \bar{\eta}_4; mn}^{(\alpha)} = \int_{\bar{\psi} \psi} \mathcal{E}_{\eta_1 \bar{\eta}_3 \psi; m}^{(\alpha)} \mathcal{F}_{\bar{\psi} \eta_2 \bar{\eta}_4; n}^{(\alpha)} , \quad (\text{B.6})$$

$$= \int_{\bar{\zeta} \zeta, \bar{\phi} \phi, \bar{\xi} \xi} \mathcal{X}_{\eta_1 \bar{\eta}_3 \zeta}^{(\alpha)} \mathcal{P}_{\bar{\zeta} \phi; m}^{(\alpha)} \mathcal{Q}_{\bar{\phi} \xi; n}^{(\alpha)} \mathcal{Y}_{\bar{\xi} \eta_2 \bar{\eta}_4}^{(\alpha)} . \quad (\text{B.7})$$

In (B.6), both \mathcal{E} and \mathcal{F} absorb the square root of the singular value in their definition. In (B.7), \mathcal{E} is further decomposed into \mathcal{X} and \mathcal{P} with \mathcal{X} absorbing the singular values and \mathcal{F} is also decomposed into \mathcal{Y} and \mathcal{Q} with \mathcal{Y} absorbing the singular values.

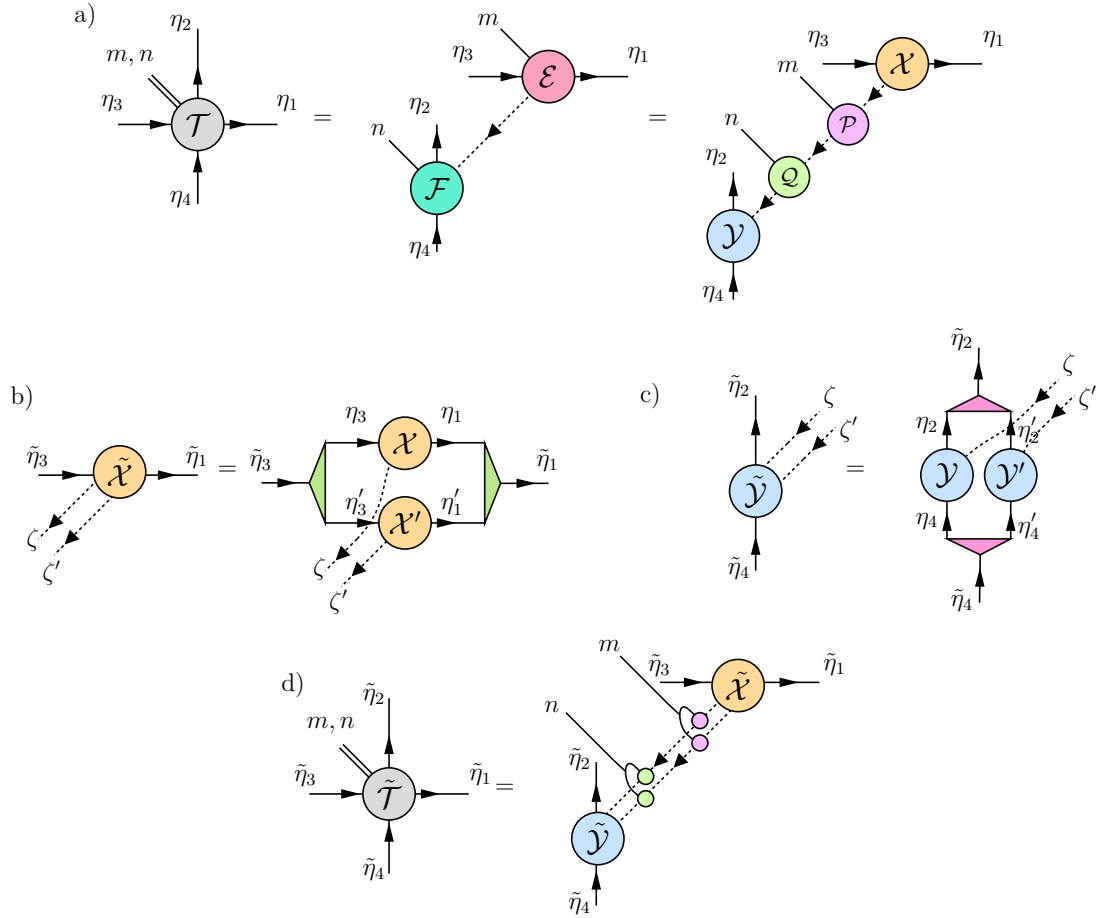


Figure 11: Schematic representation of the Grassmann HOTRG algorithm for the site tensor (3.23). a) the \mathcal{X} - \mathcal{Y} decomposition (B.7), b) $\tilde{\mathcal{X}}$ (B.14), c) $\tilde{\mathcal{Y}}$ (B.15) and d) the coarse-grained tensor $\tilde{\mathcal{T}}$ (B.16).

To merge the legs from the layer α and α' , we next define

$$\hat{\mathcal{X}}_{\bar{\eta}_3 \bar{\eta}'_3 \zeta \zeta' \eta_1 \eta'_1} = \mathcal{X}_{\eta_1 \bar{\eta}_3 \zeta}^{(\alpha)} \mathcal{X}_{\eta'_1 \bar{\eta}'_3 \zeta'}^{(\alpha')}, \quad (\text{B.8})$$

$$\hat{\mathcal{Y}}_{\bar{\eta}_4 \bar{\eta}'_4 \bar{\xi} \bar{\xi}' \eta_2 \eta'_2} = \mathcal{Y}_{\bar{\xi} \eta_2 \bar{\eta}_4}^{(\alpha)} \mathcal{Y}_{\bar{\xi}' \eta'_2 \bar{\eta}'_4}^{(\alpha')}. \quad (\text{B.9})$$

Then we form the Hermitian matrices for the isometry computation:

$$(\mathcal{M}_1)_{(\bar{\eta}_1 \bar{\eta}'_1)(\eta_1 \eta'_1)} = \int_{\bar{\eta}_3 \eta_3, \bar{\eta}'_3 \eta'_3, \bar{\zeta} \zeta, \bar{\zeta}' \zeta'} \hat{\mathcal{X}}_{(\bar{\eta}_1 \bar{\eta}'_1)(\eta_3 \eta'_3 \bar{\zeta} \bar{\zeta}')}^\dagger \hat{\mathcal{X}}_{(\bar{\eta}_3 \bar{\eta}'_3 \zeta \zeta')(\eta_1 \eta'_1)}, \quad (\text{B.10})$$

$$(\mathcal{M}_3)_{(\bar{\eta}_3 \bar{\eta}'_3)(\eta_3 \eta'_3)} = \int_{\bar{\eta}_1 \eta_1, \bar{\eta}'_1 \eta'_1, \bar{\zeta} \zeta, \bar{\zeta}' \zeta'} \hat{\mathcal{X}}_{(\bar{\eta}_3 \bar{\eta}'_3)(\zeta \zeta' \eta_1 \eta'_1)} \hat{\mathcal{X}}_{(\bar{\zeta} \bar{\zeta}' \bar{\eta}_1 \bar{\eta}'_1)(\eta_3 \eta'_3)}^\dagger, \quad (\text{B.11})$$

$$(\mathcal{M}_2)_{(\bar{\eta}_2 \bar{\eta}'_2)(\eta_2 \eta'_2)} = \int_{\bar{\eta}_4 \eta_4, \bar{\eta}'_4 \eta'_4, \bar{\xi} \xi, \bar{\xi}' \xi'} \hat{\mathcal{Y}}_{(\bar{\eta}_2 \bar{\eta}'_2)(\eta_4 \eta'_4 \xi \xi')}^\dagger \hat{\mathcal{Y}}_{(\bar{\eta}_4 \bar{\eta}'_4 \bar{\xi} \bar{\xi}')(\eta_2 \eta'_2)}, \quad (\text{B.12})$$

$$(\mathcal{M}_4)_{(\bar{\eta}_4 \bar{\eta}'_4)(\eta_4 \eta'_4)} = \int_{\bar{\eta}_2 \eta_2, \bar{\eta}'_2 \eta'_2, \bar{\xi} \xi, \bar{\xi}' \xi'} \hat{\mathcal{Y}}_{(\bar{\eta}_4 \bar{\eta}'_4)(\bar{\xi} \bar{\xi}' \eta_2 \eta'_2)} \hat{\mathcal{Y}}_{(\xi \xi' \bar{\eta}_2 \bar{\eta}'_2)(\eta_4 \eta'_4)}^\dagger. \quad (\text{B.13})$$

The unitary matrices along the same axis are then compared by their singular values as explained before. The resulting isometries $(\mathcal{U}_x)_{(\bar{\eta})(\bar{\eta}\bar{\eta}')}$ and $(\mathcal{U}_y)_{(\bar{\eta})(\bar{\eta}\bar{\eta}')}$ are then used for the truncation

$$\tilde{\mathcal{X}}_{\bar{\eta}_3 \zeta \zeta' \bar{\eta}_1} = \int_{\bar{\eta}_1 \eta_1, \bar{\eta}'_1 \eta'_1, \bar{\eta}_3 \eta_3, \bar{\eta}'_3 \eta'_3} (\mathcal{U}_x)_{(\bar{\eta}_3)(\eta_3 \eta'_3)} \hat{\mathcal{X}}_{\bar{\eta}_3 \bar{\eta}'_3 \zeta \zeta' \eta_1 \eta'_1} (\mathcal{U}_x)_{(\bar{\eta}_1 \bar{\eta}'_1)(\bar{\eta}_1)}^\dagger, \quad (\text{B.14})$$

$$\tilde{\mathcal{Y}}_{\bar{\eta}_4 \bar{\xi} \bar{\xi}' \bar{\eta}_2} = \int_{\bar{\eta}_2 \eta_2, \bar{\eta}'_2 \eta'_2, \bar{\eta}_4 \eta_4, \bar{\eta}'_4 \eta'_4} (\mathcal{U}_y)_{(\bar{\eta}_4)(\eta_4 \eta'_4)} \hat{\mathcal{Y}}_{\bar{\eta}_4 \bar{\eta}'_4 \bar{\xi} \bar{\xi}' \eta_2 \eta'_2} (\mathcal{U}_y)_{(\bar{\eta}_2 \bar{\eta}'_2)(\bar{\eta}_2)}^\dagger. \quad (\text{B.15})$$

The final coarse-grained tensor can then be constructed as

$$\tilde{\mathcal{T}}_{\bar{\eta}_1 \bar{\eta}_2 \bar{\eta}_3 \bar{\eta}_4; mn} = \int_{\substack{\bar{\zeta} \zeta, \bar{\phi} \phi, \bar{\xi} \xi, \\ \bar{\zeta}' \zeta', \bar{\phi}' \phi', \bar{\xi}' \xi'}} \tilde{\mathcal{X}}_{\bar{\eta}_3 \zeta \zeta' \bar{\eta}_1} \mathcal{P}_{\bar{\zeta} \phi; m}^{(\alpha)} \mathcal{P}_{\bar{\zeta}' \phi'; m}^{(\alpha')} \mathcal{Q}_{\bar{\phi} \xi; n}^{(\alpha)} \mathcal{Q}_{\bar{\phi}' \xi'; n}^{(\alpha')} \tilde{\mathcal{Y}}_{\bar{\eta}_4 \bar{\xi} \bar{\xi}' \bar{\eta}_2}. \quad (\text{B.16})$$

The schematic representation of $\tilde{\mathcal{X}}$, $\tilde{\mathcal{Y}}$ and $\tilde{\mathcal{T}}$ are shown in Fig. 11-b to -d. After repeating the above gHOTRG appropriate times, we can finally obtain the flavor coarse-grained tensor $\mathcal{T}''_{\psi_1 \psi_2 \bar{\psi}_3 \bar{\psi}_4; mn}$ in the right-hand side of (3.26), where we have used ψ indices instead of $\tilde{\eta}$ for clarity.

B.2 Grassmann TRG

As in the traditional TRG [17], we perform an SVD on $\mathcal{T}_{\eta_1 \eta_2 \bar{\eta}_3 \bar{\eta}_4}$ in two different ways depending on whether the tensor is located on the even or odd site of a square lattice (See Fig. 12-a.) as

$$\mathcal{T}_{\eta_1 \eta_2 \bar{\eta}_3 \bar{\eta}_4} = \int_{\bar{\xi} \xi} (\mathcal{U}_{\text{odd}})_{\eta_2 \bar{\eta}_3 \xi} (\mathcal{V}_{\text{odd}})_{\bar{\xi} \bar{\eta}_4 \eta_1} \quad (\text{B.17})$$

$$= \int_{\bar{\xi}\xi} (\mathcal{U}_{\text{even}})_{\bar{\eta}_3\bar{\eta}_4\xi} (\mathcal{V}_{\text{even}})_{\bar{\xi}\eta_1\eta_2} . \quad (\text{B.18})$$

Practically, these gSVDs are calculated in terms of the coefficient matrix representation as

$$(Q_{\text{odd}}^{(\text{m})})_{(I_2I_3)(I_4I_1)} = T_{I_1I_2I_3I_4} \sigma_{\{I_2,I_3\}} (-)^{p(I_1)} \quad (\text{B.19})$$

$$\stackrel{\text{SVD}}{=} \sum_J (U_{\text{odd}}^{(\text{m})})_{(I_2I_3)J} (V_{\text{odd}}^{(\text{m})})_{J(I_4I_1)} , \quad (\text{B.20})$$

$$(Q_{\text{even}}^{(\text{m})})_{(I_3I_4)(I_1I_2)} = T_{I_1I_2I_3I_4} \sigma_{\{I_3,I_4\}} (-)^{p(I_1)+p(I_2)} \quad (\text{B.21})$$

$$\stackrel{\text{SVD}}{=} \sum_J (U_{\text{even}}^{(\text{m})})_{(I_3I_4)J} (V_{\text{even}}^{(\text{m})})_{J(I_1I_2)} . \quad (\text{B.22})$$

where the square root of singular value matrices are absorbed into $U^{(\text{m})}$ and $V^{(\text{m})}$. Using $U^{(\text{m})}$ and $V^{(\text{m})}$, one can then obtain the blocked tensor with renormalized legs as (See Fig. 12-b.)

$$\tilde{\mathcal{T}}_{\xi_1\xi_2\bar{\xi}_3\bar{\xi}_4} = \int_{\bar{\eta}_1\eta_1,\bar{\eta}_2\eta_2,\bar{\eta}_3\eta_3,\bar{\eta}_4\eta_4} (\mathcal{U}_{\text{even}})_{\bar{\eta}_3\bar{\eta}_2\xi_2} (\mathcal{U}_{\text{odd}})_{\eta_2\bar{\eta}_1\xi_1} (\mathcal{V}_{\text{even}})_{\bar{\xi}_4\eta_1\eta_4} (\mathcal{V}_{\text{odd}})_{\bar{\xi}_3\bar{\eta}_4\eta_3} . \quad (\text{B.23})$$

For convenience, we also note the explicit form of the coefficient tensors below

$$\tilde{\mathcal{T}}_{J_1J_2J_3J_4} = \sum_{I_3I_1} U'_{I_3I_1J_1J_2} V'_{J_3J_4I_1I_3} \sigma_{I_1} \sigma_{I_3} (-)^{p(J_1)+p(J_2)} , \quad (\text{B.24})$$

$$U'_{I_3I_1J_1J_2} = \sum_{I_2} (U_{\text{even}}^{(\text{m})})_{(I_3I_2)J_2} (U_{\text{odd}}^{(\text{m})})_{(I_2I_1)J_1} \sigma_{I_2} \sigma_{\{I_3,I_2\}} \sigma_{\{I_2,I_1\}} (-)^{p(I_2)} , \quad (\text{B.25})$$

$$V'_{J_3J_4I_1I_3} = \sum_{I_4} (V_{\text{even}}^{(\text{m})})_{J_4(I_1I_4)} (V_{\text{odd}}^{(\text{m})})_{J_3(I_4I_3)} \sigma_{I_4} \sigma_{J_4} \sigma_{J_3} . \quad (\text{B.26})$$

C Adding local inter-flavor interactions

In this paper, we have considered the case in which different flavors interact through the gauge field only. However, our method can be generalized to models with local inter-flavor interactions. Here we consider the interaction term in the Lagrangian given by

$$L_x^{(\lambda)} = \sum_{I_1 \dots J_{N_f}} \lambda_{I_1 \dots I_{N_f} J_1 \dots J_{N_f}} (\psi_x^{(1)})^{I_1} \dots (\psi_x^{(N_f)})^{I_{N_f}} (\bar{\psi}_x^{(1)})^{J_1} \dots (\bar{\psi}_x^{(N_f)})^{J_{N_f}} \quad (\text{C.1})$$

with the Boltzmann weight

$$e^{-L_x^{(\lambda)}} = \sum_{I_1 \dots J_{N_f}} B_{I_1 \dots I_{N_f} J_1 \dots J_{N_f}}^{(\lambda)} (\psi_x^{(1)})^{I_1} \dots (\psi_x^{(N_f)})^{I_{N_f}} (\bar{\psi}_x^{(1)})^{J_1} \dots (\bar{\psi}_x^{(N_f)})^{J_{N_f}} . \quad (\text{C.2})$$

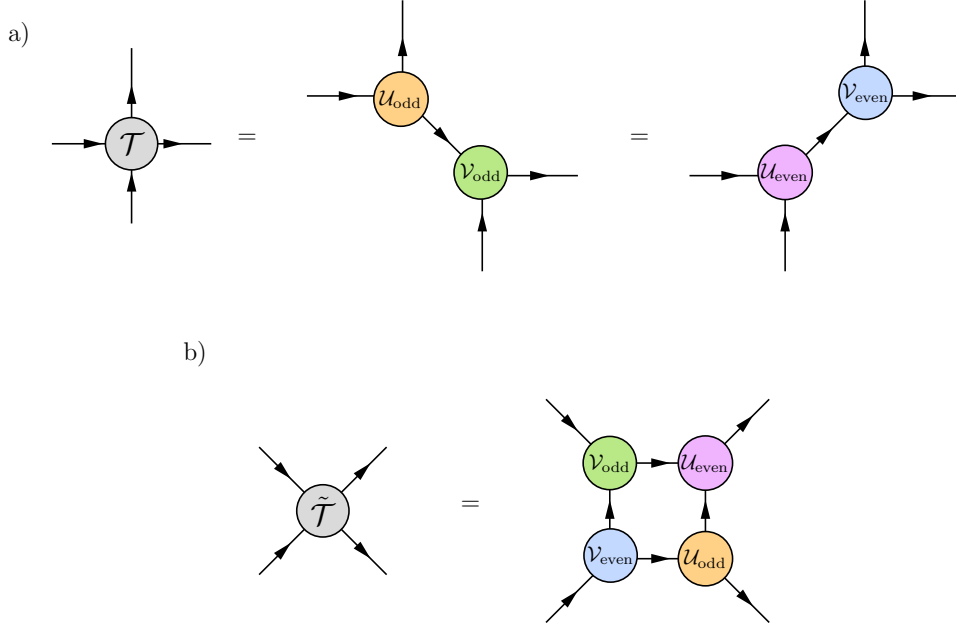


Figure 12: schematic representation of the Grassmann TRG algorithm.

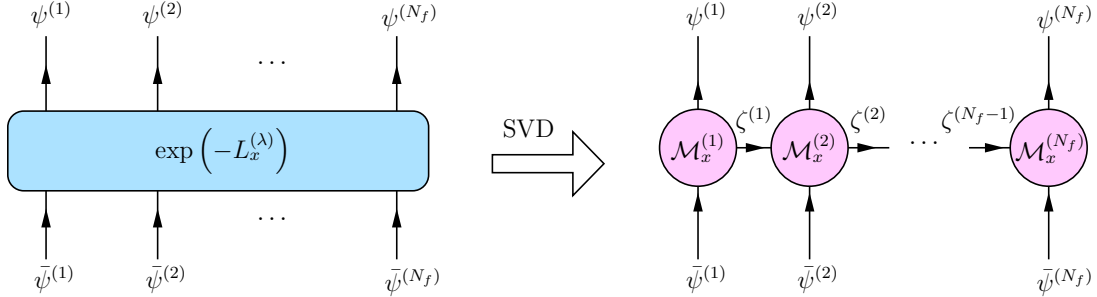


Figure 13: Decomposition of the Boltzmann weight $e^{-L_x^{(\lambda)}}$ defined in (C.2).

If we treat all the fermions as Grassmann indices, we can perform the tensor decomposition of the Boltzmann weight in the same spirit as in Ref. [49] as

$$e^{-L_x^{(\lambda)}} = \int_{\substack{\bar{\zeta}_x^{(1)} \zeta_x^{(1)}, \dots \\ \bar{\zeta}_x^{(N_f-1)} \zeta_x^{(N_f-1)}}} \mathcal{M}_{\psi_x^{(1)} \bar{\psi}_x^{(1)} \zeta_x^{(1)}}^{(1)} \mathcal{M}_{\bar{\zeta}_x^{(1)} \psi_x^{(2)} \bar{\psi}_x^{(2)} \zeta_x^{(2)}}^{(2)} \cdots \mathcal{M}_{\bar{\zeta}_x^{(N_f-1)} \psi_x^{(N_f)} \bar{\psi}_x^{(N_f)}}^{(N_f)}, \quad (\text{C.3})$$

as shown in Fig. 13.

The partition function with this interaction term now becomes

$$Z = \int_{\bar{\eta}, \bar{\zeta}, \bar{\xi}} \sum_{\{\varphi\}} \prod_{x, \alpha} \mathcal{T}_x^{(\alpha)}, \quad (\text{C.4})$$

where we have defined

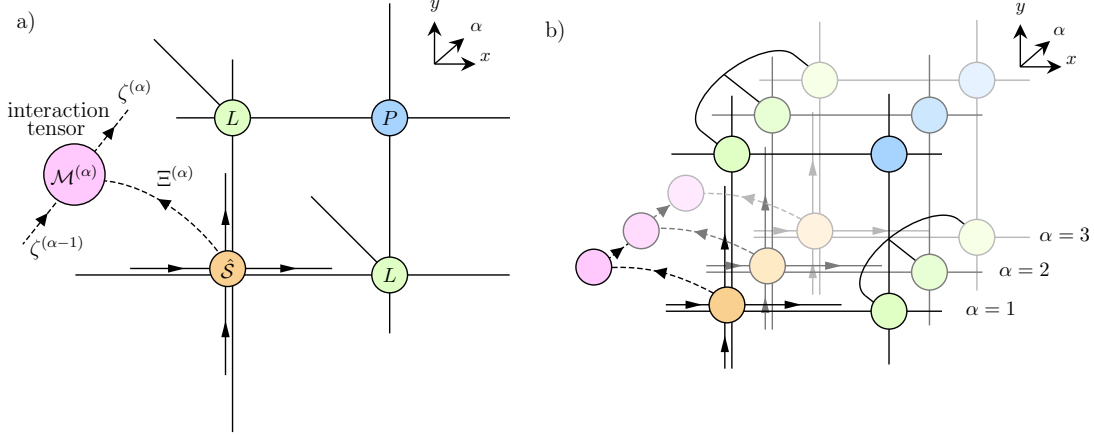


Figure 14: Connection of the tensors with the local multi-flavor interaction. a) The site tensor. b) The connection between layers corresponding to the $N_f = 3$ case.

$$\mathcal{T}_x^{(\alpha)} = P_x^{(\alpha)} \hat{S}_x^{(\alpha)} L_{x,1}^{(\alpha)} L_{x,2}^{(\alpha)} \mathcal{M}_x^{(\alpha)}, \quad (\text{C.5})$$

$$\hat{S}_x^{(\alpha)} = \int d\psi_x^{(\alpha)} d\bar{\psi}_x^{(\alpha)} e^{-\bar{\psi}_x^{(\alpha)} W_x^{(\alpha)} \psi_x^{(\alpha)} - \sum_{\pm, \nu} \{ \bar{\psi}_x^{(\alpha)} \eta_{x, \pm \nu}^{(\alpha)} - \bar{\eta}_{x \mp \hat{\nu}, \pm \nu}^{(\alpha)} H_{x \mp \hat{\nu}, \pm \nu}^{(\alpha)} \psi_x^{(\alpha)} \}} \mathcal{I}_{\bar{\psi}_x^{(\alpha)} \xi_x^{(\alpha)}} \mathcal{I}_{\bar{\xi}_x^{(\alpha)} \psi_x^{(\alpha)}}, \quad (\text{C.6})$$

$$\mathcal{I}_{\bar{\psi} \xi} = \sum_I \sigma_I \bar{\psi}^I \xi^I. \quad (\text{C.7})$$

The difference between this result and the original one in (2.14)-(2.17) is that we now have the interaction tensor $\mathcal{M}_{\bar{\zeta}^{(\alpha-1)} \xi^{(\alpha)} \bar{\xi}^{(\alpha)} \zeta^{(\alpha)}}$, which is connected with $\hat{S}^{(\alpha)}$ through two extra connection tensors $\mathcal{I}_{\bar{\psi}^{(\alpha)} \xi^{(\alpha)}}$ and $\mathcal{I}_{\bar{\xi}^{(\alpha)} \psi^{(\alpha)}}$. These connection tensors are actually the Grassmann identity matrices which have the property that their contraction with any Grassmann tensor always gives the same tensor. The legs $(\bar{\xi}^{(\alpha)}, \xi^{(\alpha)})$ can be merged into a single fermion $\Xi^{(\alpha)}$ with the prescription (A.17)-(A.18). The connection of the interaction tensor \mathcal{M} with \hat{S} on the lattice is shown in Fig. 14.

Since the general structure of the tensor network is similar to that in Fig. 1, appropriate compression and coarse-graining techniques can be straightforwardly applied to this site tensor.

References

- [1] G. Parisi, *On complex probabilities*, *Phys. Lett. B* **131** (1983) 393.

- [2] K. Nagata, J. Nishimura and S. Shimasaki, *Argument for justification of the complex Langevin method and the condition for correct convergence*, *Phys. Rev. D* **94** (2016) 114515 [1606.07627].
- [3] G. Aarts, E. Seiler and I.-O. Stamatescu, *The Complex Langevin method: When can it be trusted?*, *Phys. Rev. D* **81** (2010) 054508 [0912.3360].
- [4] E. Seiler, D. Sexty and I.-O. Stamatescu, *Gauge cooling in complex Langevin for QCD with heavy quarks*, *Phys. Lett. B* **723** (2013) 213 [1211.3709].
- [5] Y. Ito and J. Nishimura, *The complex Langevin analysis of spontaneous symmetry breaking induced by complex fermion determinant*, *JHEP* **12** (2016) 009 [1609.04501].
- [6] E. Picard and G. Simart, *Theorie des fonctions algebriques de deux variables independantes. Tome I*, (1897) .
- [7] S. Lefschetz, *L'analysis situs et la geometrie algebrique*, (1924) .
- [8] E. Witten, *Analytic Continuation Of Chern-Simons Theory*, *AMS/IP Stud. Adv. Math.* **50** (2011) 347 [1001.2933].
- [9] E. Witten, *A New Look At The Path Integral Of Quantum Mechanics*, 1009.6032.
- [10] A. Alexandru, G. Basar, P.F. Bedaque and N.C. Warrington, *Tempered transitions between thimbles*, *Phys. Rev. D* **96** (2017) 034513 [1703.02414].
- [11] A. Matsumoto, K. Hatakeyama, M. Hirasawa, M. Honda, Y. Ito, J. Nishimura et al., *A new technique for solving the freezing problem in the complex Langevin simulation of 4D SU(2) gauge theory with a theta term*, in *38th International Symposium on Lattice Field Theory*, 12, 2021 [2112.01805].
- [12] G. Fujisawa, J. Nishimura, K. Sakai and A. Yosprakob, *Backpropagating Hybrid Monte Carlo algorithm for fast Lefschetz thimble calculations*, *JHEP* **04** (2022) 179 [2112.10519].
- [13] A. Gocksch, P. Rossi and U.M. Heller, *QUENCHED HADRONIC SCREENING LENGTHS AT HIGH TEMPERATURE*, *Phys. Lett. B* **205** (1988) 334.
- [14] A. Gocksch, *SIMULATING LATTICE QCD AT FINITE DENSITY*, *Phys. Rev. Lett.* **61** (1988) 2054.

- [15] K. Langfeld, B. Lucini and A. Rago, *The density of states in gauge theories*, *Phys. Rev. Lett.* **109** (2012) 111601 [1204.3243].
- [16] K. Okunishi, T. Nishino and H. Ueda, *Developments in the Tensor Network — from Statistical Mechanics to Quantum Entanglement*, *J. Phys. Soc. Jap.* **91** (2022) 062001 [2111.12223].
- [17] M. Levin and C.P. Nave, *Tensor renormalization group approach to 2D classical lattice models*, *Phys. Rev. Lett.* **99** (2007) 120601 [cond-mat/0611687].
- [18] G. Evenbly and G. Vidal, *Tensor network renormalization*, *Phys. Rev. Lett.* **115** (2015) 180405.
- [19] M. Hauru, C. Delcamp and S. Mizera, *Renormalization of tensor networks using graph independent local truncations*, *Phys. Rev. B* **97** (2018) 045111 [1709.07460].
- [20] D. Adachi, T. Okubo and S. Todo, *Bond-weighted Tensor Renormalization Group*, 2011.01679.
- [21] Z.Y. Xie, J. Chen, M.P. Qin, J.W. Zhu, L.P. Yang and T. Xiang, *Coarse-graining renormalization by higher-order singular value decomposition*, *Phys. Rev. B* **86** (2012) 045139.
- [22] D. Adachi, T. Okubo and S. Todo, *Anisotropic Tensor Renormalization Group*, *Phys. Rev. B* **102** (2020) 054432 [1906.02007].
- [23] D. Kadoh and K. Nakayama, *Renormalization group on a triad network*, 1912.02414.
- [24] R. Sakai, S. Takeda and Y. Yoshimura, *Higher order tensor renormalization group for relativistic fermion systems*, *PTEP* **2017** (2017) 063B07 [1705.07764].
- [25] Z.-C. Gu, F. Verstraete and X.-G. Wen, *Grassmann tensor network states and its renormalization for strongly correlated fermionic and bosonic states*, 1004.2563.
- [26] Z.-C. Gu, *Efficient simulation of Grassmann tensor product states*, *Phys. Rev. B* **88** (2013) 115139 [1109.4470].
- [27] Y. Shimizu and Y. Kuramashi, *Grassmann tensor renormalization group approach to one-flavor lattice Schwinger model*, *Phys. Rev. D* **90** (2014) 014508 [1403.0642].
- [28] S. Akiyama and D. Kadoh, *More about the Grassmann tensor renormalization group*, *JHEP* **10** (2021) 188 [2005.07570].

- [29] K. Nakayama, *Randomized higher-order tensor renormalization group*, 2307.14191.
- [30] D. Perez-Garcia, F. Verstraete, M.M. Wolf and J.I. Cirac, *Matrix product state representations*, 2007.
- [31] R.J. Baxter, *Dimers on a rectangular lattice*, *Journal of Mathematical Physics* **9** (1968) 650 [<https://doi.org/10.1063/1.1664623>].
- [32] S.R. White, *Density matrix formulation for quantum renormalization groups*, *Phys. Rev. Lett.* **69** (1992) 2863.
- [33] T. Nishino and K. Okunishi, *Corner transfer matrix renormalization group method*, *Journal of the Physical Society of Japan* **65** (1996) 891 [<https://doi.org/10.1143/JPSJ.65.891>].
- [34] T. Nishino and K. Okunishi, *Corner transfer matrix algorithm for classical renormalization group*, *Journal of the Physical Society of Japan* **66** (1997) 3040 [<https://doi.org/10.1143/JPSJ.66.3040>].
- [35] T. Nishino and K. Okunishi, *A density matrix algorithm for 3d classical models*, *Journal of the Physical Society of Japan* **67** (1998) 3066 [<https://doi.org/10.1143/JPSJ.67.3066>].
- [36] Y. Kuramashi and Y. Yoshimura, *Tensor renormalization group study of two-dimensional $U(1)$ lattice gauge theory with a θ term*, *JHEP* **04** (2020) 089 [1911.06480].
- [37] M. Fukuma, D. Kadoh and N. Matsumoto, *Tensor network approach to two-dimensional Yang–Mills theories*, *PTEP* **2021** (2021) 123B03 [2107.14149].
- [38] M. Hirasawa, A. Matsumoto, J. Nishimura and A. Yosprakob, *Tensor renormalization group and the volume independence in 2D $U(N)$ and $SU(N)$ gauge theories*, *JHEP* **12** (2021) 011 [2110.05800].
- [39] A. Bazavov, S. Catterall, R.G. Jha and J. Unmuth-Yockey, *Tensor renormalization group study of the non-Abelian Higgs model in two dimensions*, *Phys. Rev. D* **99** (2019) 114507 [1901.11443].
- [40] Y. Shimizu and Y. Kuramashi, *Critical behavior of the lattice Schwinger model with a topological term at $\theta = \pi$ using the Grassmann tensor renormalization group*, *Phys. Rev. D* **90** (2014) 074503 [1408.0897].

- [41] Y. Shimizu and Y. Kuramashi, *Berezinskii-Kosterlitz-Thouless transition in lattice Schwinger model with one flavor of Wilson fermion*, *Phys. Rev. D* **97** (2018) 034502 [1712.07808].
- [42] J. Bloch and R. Lohmayer, *Grassmann higher-order tensor renormalization group approach for two-dimensional strong-coupling QCD*, *Nucl. Phys. B* **986** (2023) 116032 [2206.00545].
- [43] T. Kuwahara and A. Tsuchiya, *Toward tensor renormalization group study of three-dimensional non-Abelian gauge theory*, *PoS LATTICE2022* (2023) 021.
- [44] S. Akiyama and Y. Kuramashi, *Tensor renormalization group study of (3+1)-dimensional \mathbb{Z}_2 gauge-Higgs model at finite density*, *JHEP* **05** (2022) 102 [2202.10051].
- [45] S. Akiyama and Y. Kuramashi, *Critical endpoint of (3+1)-dimensional finite density \mathbb{Z}_3 gauge-Higgs model with tensor renormalization group*, 2304.07934.
- [46] D.B. Kaplan, *A Method for simulating chiral fermions on the lattice*, *Phys. Lett. B* **288** (1992) 342 [hep-lat/9206013].
- [47] D.B. Kaplan, *Chiral fermions on the lattice*, *Nucl. Phys. B Proc. Suppl.* **30** (1993) 597.
- [48] I. Hip, C.B. Lang and R. Teppner, *Chiral symmetry in the two flavor lattice Schwinger model*, *Nucl. Phys. B Proc. Suppl.* **63** (1998) 682 [hep-lat/9709030].
- [49] S. Akiyama, *Matrix product decomposition for two- and three-flavor Wilson fermion: benchmark results in the lattice Gross-Neveu model at finite density*, 2304.01473.
- [50] L. De Lathauwer, B. De Moor and J. Vandewalle, *A multilinear singular value decomposition*, *SIAM Journal on Matrix Analysis and Applications* **21** (2000) 1253 [https://doi.org/10.1137/S0895479896305696].
- [51] J. Gao, W. Ji, F. Chang, S. Han, B. Wei, Z. Liu et al., *A systematic survey of general sparse matrix-matrix multiplication*, *ACM Comput. Surv.* **55** (2023) .
- [52] A. Yosprakob, *GrassmannTN: a Python package for Grassmann tensor network computation* <https://github.com/ayosprakob/grassmanntn>, .
- [53] T.D. Cohen, *Functional integrals for QCD at nonzero chemical potential and zero density*, *Phys. Rev. Lett.* **91** (2003) 222001 [hep-ph/0307089].

- [54] S. Akiyama, *Bond-weighting method for the Grassmann tensor renormalization group*, *JHEP* **11** (2022) 030 [2208.03227].
- [55] A.J. Ferris, *Unbiased monte carlo for the age of tensor networks*, 2015.
- [56] W. Huggins, C.D. Freeman, M. Stoudenmire, N.M. Tubman and K.B. Whaley, *Monte carlo tensor network renormalization*, 2017.
- [57] E. Arai, H. Ohki, S. Takeda and M. Tomii, *All-mode renormalization for tensor network with stochastic noise*, *Phys. Rev. D* **107** (2023) 114515 [2211.13107].